

# Wave scattering in layered orthotropic media I: a stable PML and a high-accuracy boundary integral equation method

Yong Gao<sup>1</sup> and Wangtao Lu<sup>2</sup>

March 7, 2022

## Abstract

In anisotropic media, the standard perfectly matched layer (PML) technique suffers irrevocable instability in terminating the unbounded problem domains. It remains an open question whether a stable PML-like absorbing boundary condition exists. For wave scattering in a layered orthotropic medium, this question is affirmatively answered for the first time in this paper. In each orthotropic medium, the permittivity tensor uniquely determines a change of coordinates, that transforms the governing anisotropic Helmholtz equation into an isotropic Helmholtz equation in the new coordinate system. This leads us to propose a novel Sommerfeld radiation condition (SRC) to rigorously characterize outgoing waves in the layered orthotropic medium. Naturally, the SRC motivates a regionalized PML (RPML) to truncate the scattering problem, in the sense that a standard PML is set up in the new coordinate system in each orthotropic region. It is revealed that the RPML is unconditionally stable compared with the unstable uniaxial PML. A high-accuracy boundary integral equation (BIE) method is developed to solve the resulting boundary value problem. Numerical experiments are carried out to validate the stability of the RPML and the accuracy of the BIE method, showing exponentially decaying truncation errors as the RPML parameters increase.

## 1 Introduction

Wave scattering problems arise from a wide range of realistic applications [9] including optics, radar, remote sensing, seismology, etc. Efficient and accurate numerical methods are highly desirable in related simulations. One essential difficulty among many others is how to accurately truncate the unbounded problem domains in the

---

<sup>1</sup>School of Mathematical Sciences, Zhejiang University, Hangzhou 310027, China. Email: xz-gaoyong@126.com.

<sup>2</sup>Corresponding author. School of Mathematical Sciences, Zhejiang University, Hangzhou 310027, China. Email: wangtaolu@zju.edu.cn. This author is partially supported by NSFC Grant 12174310 and by NSF of Zhejiang Province for Distinguished Young Scholars (LR21A010001).

first place. Coined and proposed by Berenger [3] in 1994, the perfectly matched layer (PML) technique has since then become a widespread truncation approach, due to its nearly zero reflection, easy implementation, and friendly incorporation into standard numerical methods [19, 17]. Originally, PML was used to terminate waves in homogeneous and isotropic background media, and subsequently, has so far been successfully extended to more complicated backgrounds, such as layered [15, 16] and periodic [7, 21] structures, still isotropic though.

In contrast, significant difficulty arises in the extension of PML to anisotropic backgrounds, as reported in the literature [2, 18, 20, 5]. Roughly speaking, PML is only able to absorb waves with outgoing group velocities, but cannot work for anisotropic media with two group velocities of different signs, e.g., in elastodynamics, since waves can even exponentially blow up in a PML region. Bécache et al. [2] rigorously studied the instability of PML in the time domain of elastic waves in anisotropic media, and derived a stability condition of the PML. Even worse, they further pointed out that PML for electro-magnetic or acoustic waves in orthotropic media is unconditionally unstable. To circumvent PML, Bonnet Ben-Dhia et al. [5] developed a half-space matching method to solve an acoustic wave scattering problem in an orthotropic medium with a bounded obstacle. By using analytic integral representations in half spaces surrounding the obstacle, they found an alternative artificial boundary condition on the edges of the half spaces to truncate the unbounded domain. Nevertheless, this boundary condition is not quite easy to implement compared with PML. Consequently, an attractive but still open question is: Can we find a stable PML-like absorbing boundary condition in anisotropic media? Motivated by this, this paper studies a TM-polarized electro-magnetic wave propagating in a two-dimensional (2D) two-layer orthotropic medium, and gives an affirmative answer to the question. We note that the structure in [5] is a special case of our layered structure if the two layers have the same permittivity tensor.

To design a PML-like absorbing layer, the primary task is to understand the radiation behavior of the total wave field, the nonzero component of the magnetic field, at infinity. To achieve this, in either orthotropic layer, we elaborately choose a special change of coordinates to transform the 2D governing equation, an anisotropic Helmholtz equation, into an isotropic Helmholtz equation. Unlike the usual transition matrix for orthotropic media [11], our transition matrix differs by an orthogonal matrix multiplier, which uniquely depends on the anisotropy of the medium. Such a special choice makes the method of Fourier transform applicable to determine the background Green's function. By studying the radiation behavior of the Green's function at infinity and by establishing the fundamental Green's representation formula, we are able to propose a novel Sommerfeld radiation condition (SRC) for the total wave field, to define what an outgoing wave is in orthotropic media rigorously, and to determine the far-field pattern of any outgoing wave conveniently. Certainly, the Green's representation formula directly induces an exact transparent boundary condition to truncate the unbounded domain, but rapidly evaluating the costly background Green's function and its derivatives requires carefully designed algorithms [6].

Instead, the SRC motivates us to design a regionalized PML (RPML) to truncate the unbounded domain, in the sense that a standard PML is set up regionally in the

new coordinate system in either orthotropic layer. The new RPML inherits all the advantages of the classical PML, and more importantly, it is unconditionally stable so that all standard numerical methods can be incorporated readily. To design a high-accuracy solver, we adopt our previously developed PML-based boundary integral equation (BIE) method [15]. Numerical experiments are carried out to validate the stability of the RPML and the high-accuracy of the BIE method. Numerical results show that the truncation error due to the RPML decays exponentially as the RPML parameters increase.

The rest of this paper is organized as follows. In section 2, we present a mathematical formulation and propose a radiation condition for the scattering problem. In section 3, we apply the method of Fourier transform to compute the background Green's function and study its asymptotic behavior at infinity. In section 4, we derive the Green's representation formula and the far-field pattern of an outgoing wave. In section 5, we present the setup of an RPML and the implementation of a high-accuracy BIE method, and analyze the stability of the RPML. In section 6, we study several numerical examples. In section 7, we conclude this paper and present some potential extensions of the RPML technique.

## 2 Problem formulation

Let  $(x_1, x_2, x_3)^T$  denote the Cartesian coordinate system of the three-dimensional space  $\mathbb{R}^3$ . As shown in Figure 1, two homogeneous and orthotropic media, which

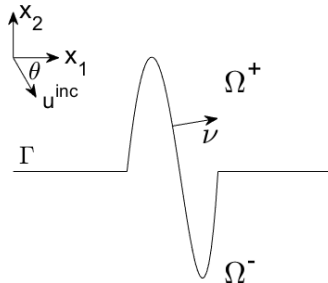


Figure 1: Profile of a 2D two-layer orthotropic medium. A locally perturbed straight line  $\Gamma$  separate two unbounded regions  $\Omega^+$  and  $\Omega^-$ ,  $\theta$  indicates the incident angle of a plane incident wave  $u^{\text{inc}}$ , and  $\nu$  is the unit normal vector of  $\Gamma$  towards  $\Omega^+$ .

are invariant in the  $x_3$ -direction, occupy two locally perturbed half planes  $\Omega^+$  and  $\Omega^-$ , respectively, in the  $x_1Ox_2$ -plane. The permittivities in  $\Omega^\pm$  are characterized by the following two positive definite tensors

$$\epsilon^\pm = \begin{bmatrix} \epsilon_{11}^\pm & \epsilon_{12}^\pm & 0 \\ \epsilon_{21}^\pm & \epsilon_{22}^\pm & 0 \\ 0 & 0 & \epsilon_{33}^\pm \end{bmatrix},$$

respectively. In this paper, we assume that the locally perturbed straight line  $\Gamma$  separating  $\Omega^\pm$  is on  $x_2 = 0$  and is piecewise smooth.

A generic time-harmonic electro-magnetic (EM) field propagating in  $\Omega^\pm$  is governed by Maxwell's equations:

$$\nabla_3 \times \mathbf{E} - \mathbf{i}k_0 \mathbf{H} = 0, \quad (1)$$

$$\nabla_3 \times \mathbf{H} + \mathbf{i}k_0 \epsilon(x) \mathbf{E} = 0, \quad (2)$$

where  $\nabla_3 = (\partial_{x_1}, \partial_{x_2}, \partial_{x_3})^T$ ,  $x = (x_1, x_2)^T$ ,  $\mathbf{E}$  is the total electric field,  $\mathbf{H}$  is the (properly scaled) total magnetic field,  $k_0 = \frac{2\pi}{\lambda}$  is the free-space wavenumber,  $\lambda$  is the free-space wavelength, and

$$\epsilon(x) := [\epsilon_{ij}(x)]_{3 \times 3} = \begin{cases} \epsilon^+, & x \in \Omega^+, \\ \epsilon^-, & x \in \Omega^-. \end{cases} \quad (3)$$

Such vectorial equations can be further simplified if the EM field possesses certain polarization. In this paper, we consider TM polarization only, i.e.,  $\mathbf{H} = (0, 0, u^{\text{tot}})^T$  where the nonzero function  $u^{\text{tot}}$  is assumed to be  $x_3$ -independent. Since

$$\nabla_3 \times [\epsilon(x)^{-1} \nabla_3 \times \mathbf{H}] - k_0^2 \mathbf{H} = 0,$$

$u^{\text{tot}}$  satisfies the following anisotropic Helmholtz equation,

$$\nabla \cdot (M(x) \nabla u^{\text{tot}}) + k_0^2 u^{\text{tot}} = 0, \quad (4)$$

on  $\mathbb{R}^2 \setminus \Gamma$ , where  $\nabla = (\partial_{x_1}, \partial_{x_2})^T$ ,

$$M(x) = \frac{1}{\epsilon_{11}(x)\epsilon_{22}(x) - \epsilon_{12}(x)^2} \begin{bmatrix} \epsilon_{11}(x) & \epsilon_{12}(x) \\ \epsilon_{12}(x) & \epsilon_{22}(x) \end{bmatrix}$$

is positive definite for any  $x \notin \Gamma$ . Across  $\Gamma$ , the following continuous condition

$$[u^{\text{tot}}]_{\text{j}} = [\nu \cdot M \nabla u^{\text{tot}}]_{\text{j}} = 0, \quad (5)$$

holds, where  $\nu$  denotes the unit normal vector of  $\Gamma$  towards  $\Omega^+$ , and  $[\cdot]_{\text{j}}$  indicates the jump of the quantity.

For  $x \in \Omega^\pm$ , let  $M_\pm = M(x)$ ,

$$M_\pm^{-1/2} = \begin{bmatrix} a_{11,\pm} & a_{12,\pm} \\ a_{12,\pm} & a_{22,\pm} \end{bmatrix} \quad (6)$$

be their inverse square roots, and

$$Q_\pm = \frac{1}{\alpha_\pm} \begin{bmatrix} a_{11,\pm} & a_{12,\pm} \\ -a_{12,\pm} & a_{11,\pm} \end{bmatrix} \quad (7)$$

be two related orthogonal matrices, where  $\alpha_\pm = \sqrt{a_{11,\pm}^2 + a_{12,\pm}^2} > 0$ . To uniquely determine  $u^{\text{tot}}$ , we need a proper radiation condition at infinity, and this relies on a precise definition of outgoing waves, as shown below.

**Definition 2.1.** Let  $B_R = \{x : |x| < R\}$  for any  $R > 0$ . A wave field  $u(x)$  is said to be outgoing in  $\Omega^\pm$  if for sufficiently large  $R$ ,  $u \in C^2(\Omega^\pm \setminus \overline{B_R})$  satisfies (4) on  $\Omega^\pm \setminus \overline{B_R}$  and (5) across  $\Gamma \setminus \overline{B_R}$ , and if  $U_\pm(X) = u(M_\pm^{1/2} Q_\pm^T X)$  satisfy the following half-plane Sommerfeld radiation condition (hpSRC)

$$\lim_{|X| \rightarrow \infty} \sqrt{|X|} \left( \frac{\partial}{\partial |X|} - \mathbf{i}k_0 \right) U_\pm(X) = 0, \quad \pm X_2 > 0, \quad (8)$$

uniformly in all directions  $X/|X| \in \{(\cos \beta, \sin \beta) : 0 \leq \pm \beta \leq \pi\}$ , where  $X = (X_1, X_2)^T$  indicates a new coordinate system via  $X = Q_\pm M_\pm^{-1/2} x$ .

The outgoing behavior of  $u$ , if satisfying (8), shall be justified later in Section 4. We make some remarks below.

**Remark 2.1.** The transition matrices  $Q_\pm M_\pm^{-1/2}$  can directly transform the anisotropic Helmholtz equation (4) on  $\Omega^\pm \setminus \overline{B_R}$  to the following isotropic Helmholtz equation

$$\Delta_X U_\pm(X) + k_0^2 U_\pm(X) = 0, \quad (9)$$

where  $\Delta_X = \sum_{j=1}^2 \partial_{X_j}^2$ . Therefore, it is natural to use the hpSRC (8) in the  $X$ -coordinate system to characterize outgoing waves in  $\Omega^\pm$ . Note that the two matrices  $Q_\pm M_\pm^{-1/2}$  are different so that the hpSRC (8) holds in two different coordinate systems.

**Remark 2.2.** The orthogonal matrices  $Q_\pm$  in fact can be replaced by any two other orthogonal matrices to keep the resulting Helmholtz equations isotropic. Nevertheless, we choose (7) since  $Q_\pm M_\pm^{-1/2}$  are upper triangular so that the horizontal  $x_2$ -axis is exactly the horizontal  $X_2$ -axis. Thus,  $c \cdot Q_\pm M_\pm^{-1/2}$  for any  $c > 0$  can be an acceptable choice. As we shall see, such a choice of  $Q_\pm$  is essential in computing the background Green's functions and in the setup of an RPML.

Certainly, it is inaccurate to directly assume that  $u^{\text{tot}}$  is outgoing without considering the incident part of  $u^{\text{tot}}$ . For simplicity, we shall assume that the incident wave is specified in  $\Omega^+$  only and that  $M_+$  is the  $2 \times 2$  identity matrix  $I_2$ . According to Remark 2.1, if  $M_+ \neq I_2$ , we use  $Q_+ M_+^{-1/2} x$  as the new two-dimensional (2D) coordinate system in the  $x_1 O x_2$ -plane so that  $u^{\text{tot}}$  satisfies (4) but with  $M(x)$  replaced by  $Q_+ M_+^{-1/2} M(x) M_+^{-1/2} Q_+^T$ . Thus, we can specify incident waves of simple forms in  $\Omega^+$ . From now on, we shall always identify  $X$  as  $Q_- M_-^{-1/2} x$  and  $x$  as  $M_-^{1/2} Q_-^T X$  when  $x \in \Omega^-$ , and for a generic domain  $\Omega \subset \Omega^-$ , we shall call  $\Omega_N$  the image of  $\Omega$  if  $\Omega_N = \{X = Q_- M_-^{-1/2} x : x \in \Omega\}$ , and hence shall call  $\Omega$  the preimage of  $\Omega_N$ .

In this paper, we consider only plane and cylindrical incident waves, and they are separately discussed below. For a plane incident wave  $u^{\text{inc}}(x; \theta) = e^{\mathbf{i}k_0(\cos \theta x_1 - \sin \theta x_2)}$ ,  $\theta \in (0, \pi)$ , specified in  $\Omega^+$ , we distinguish two cases. If  $\Gamma$  is the unperturbed straight line  $x_2 = 0$ , then the total field, referred to as the background solution  $u_b^{\text{tot}}(x; \theta)$ , and can be predetermined by the method of Fourier transform; its closed form is presented in (32) and (33) in Section 3.2. In general, if  $\Gamma$  is a locally-perturbed straight line, we enforce the following radiation condition

$$\text{(RC1):} \quad u^{\text{tot}} - u_b^{\text{tot}} \text{ is outgoing in } \Omega^\pm.$$

For a cylindrical incident wave  $u^{\text{inc}}(x; x^*) = \frac{i}{4} H_0^{(1)}(k_0|x-x^*|)$  where  $x^* = (x_1^*, x_2^*)^T \in \Omega^+$  denotes the exciting source point, the right-hand side of (4) should be replaced by  $-\delta(x-x^*)$ . Thus,  $u^{\text{tot}}(x; x^*)$  represents the Green's function excited by the source point  $x^*$ . The background solution, the Green's function  $u_b^{\text{tot}}(x; x^*)$ , for the unperturbed case  $\Gamma = \{x : x_2 = 0\}$ , can again be predetermined; see Section 3.1 for details. In the locally perturbed case, one can still enforce (RC1), but it is practically more efficient to enforce the following radiation condition

$$\text{(RC2):} \quad u^{\text{tot}} \text{ is outgoing in } \Omega^\pm,$$

since  $u_b^{\text{tot}}$  is not involved. The equivalence of (RC1) and (RC2) for cylindrical-wave incidences shall be justified in Corollary 3.1.

The objective of this paper is to develop an efficient numerical method to compute  $u^{\text{tot}}$  governed by (4), (5), and one of the two radiation conditions (RC1) and (RC2) depending on the type of the incidence. To achieve this, it is clear that the background solutions  $u_b^{\text{tot}}$  should be computed in advance, and this is the main content of the next section.

### 3 Background solutions

In this section, we assume  $\Gamma = \{x \in \mathbb{R}^2 : x_2 = 0\}$  so that  $\Omega_\pm = \mathbb{R}_\pm^2 := \{x \in \mathbb{R}^2 : \pm x_2 > 0\}$ . We shall use the method of Fourier transform to compute the background solutions  $u_b^{\text{tot}}$  for plane and cylindrical incident waves.

#### 3.1 Cylindrical incident wave

By convention, it is more appropriate to use  $G(x; x^*)$  instead of  $u_b^{\text{tot}}(x; x^*)$  to denote the background Green's function. We consider first the case  $x^* \in \mathbb{R}_+^2$ , i.e.,  $x_2^* > 0$ . Recall that  $\alpha_- = \sqrt{a_{11,-}^2 + a_{12,-}^2}$ , and that we have assumed  $M_+ = I_2$ . According to Remark 2.1,  $G(x; x^*)$  satisfies

$$\Delta G(x; x^*) + k_0^2 G(x; x^*) = -\delta(x-x^*), \quad x_2 > 0, \quad (10)$$

$$\Delta_X G_-(X; x^*) + k_0^2 G_-(X; x^*) = 0, \quad X_2 < 0, \quad (11)$$

$$G(x; x^*) = G_-(X; x^*), \quad \partial_{x_2} G(x; x^*) = \alpha_- \sqrt{|M_-|} \partial_{X_2} G_-(X; x^*), \quad x_2 = 0 = X_2, \quad (12)$$

where  $G_-(X; x^*) = G(M_-^{1/2} Q_-^T X; x^*)$ ,  $|M_-|$  denotes the determinant of  $M_-$ , (12) is derived from (5). Note that  $x_2 < 0$  and  $X_2 < 0$  represent the same lower-half plane  $\mathbb{R}_-^2$ , i.e., the image of  $\mathbb{R}_-^2$  is itself. Let

$$\hat{G}(x_2; x^*, \xi) = \int_{-\infty}^{\infty} G(x; x^*) e^{i\xi x_1} dx_1 \quad \text{and} \quad \hat{G}_-(X_2; x^*, \xi) = \int_{-\infty}^{\infty} G_-(X; x^*) e^{i\xi X_1} dX_1$$

be the one-dimensional Fourier transforms of  $G$  and  $G_-$  w.r.t  $x_1$  and  $X_1$  variables, respectively. The governing ordinary differential equations of  $\hat{G}$  and  $\hat{G}_-$  are

$$\hat{G}'''(x_2; x^*, \xi) + \mu(\xi)^2 \hat{G}(x_2; \xi) = -e^{i\xi x_1^*} \delta(x_2 - x_2^*), \quad x_2 > 0, \quad (13)$$

$$\hat{G}''_-(X_2; x^*, \xi) + \mu(\xi)^2 \hat{G}_-(X_2; x^*, \xi) = 0, \quad X_2 < 0, \quad (14)$$

where  $\mu(\xi) = \sqrt{k_0^2 - \xi^2}$ . Throughout this paper, we use the negative real axis as the branch cut of the square-root function  $\sqrt{\cdot}$  to limit its argument onto  $(-\pi/2, \pi/2]$ . Thus, we seek  $\hat{G}$  and  $\hat{G}_-$  in the form of

$$\hat{G}(x_2; x^*, \xi) = \frac{\mathbf{i}}{2\mu(\xi)} e^{\mathbf{i}\mu(\xi)|x_2 - x_2^*| + \mathbf{i}\xi x_1^*} + A(\xi) e^{\mathbf{i}\mu(\xi)x_2}, \quad (15)$$

$$\hat{G}_-(X_2; x^*, \xi) = B(\xi) e^{-\mathbf{i}\mu(\xi)X_2}, \quad (16)$$

where we have disregarded the downgoing wave  $e^{-\mathbf{i}\mu x_2}$  in  $\hat{G}$  and the upgoing wave  $e^{\mathbf{i}\mu X_2}$  in  $\hat{G}_-$ . The continuous condition (12) implies

$$\hat{G}_-(0; x^*, \xi) = \alpha_- \hat{G}(0; x^*, \alpha_- \xi), \quad \hat{G}'_-(0; x^*, \xi) = |M_-|^{-1/2} \hat{G}'(0; x^*, \alpha_- \xi), \quad (17)$$

so that

$$A(\alpha_- \xi) + \frac{\mathbf{i}}{2\mu(\alpha_- \xi)} e^{\mathbf{i}\mu(\alpha_- \xi)x_2^* + \mathbf{i}\alpha_- \xi x_1^*} = \frac{1}{\alpha_-} B(\xi),$$

$$A(\alpha_- \xi) - \frac{\mathbf{i}}{2\mu(\alpha_- \xi)} e^{\mathbf{i}\mu(\alpha_- \xi)x_2^* + \mathbf{i}\alpha_- \xi x_1^*} = -\frac{|M_-|^{1/2} \mu(\xi)}{\mu(\alpha_- \xi)} B(\xi).$$

Solving the above linear system gives rise to

$$A(\xi) = \frac{\mathbf{i}(\mu(\xi) - |M_-|^{1/2} \alpha_- \mu(\alpha_-^{-1} \xi))}{2\mu(\xi)(\mu(\xi) + |M_-|^{1/2} \alpha_- \mu(\alpha_-^{-1} \xi))} e^{\mathbf{i}\mu(\xi)x_2^* + \mathbf{i}\xi x_1^*}, \quad (18)$$

$$B(\xi) = \frac{\alpha_- \mathbf{i}}{\mu(\alpha_- \xi) + |M_-|^{1/2} \alpha_- \mu(\xi)} e^{\mathbf{i}\mu(\alpha_- \xi)x_2^* + \mathbf{i}\alpha_- \xi x_1^*}. \quad (19)$$

Thus, inverse Fourier transforming  $\hat{G}$ , we obtain for  $x \in \mathbb{R}_+^2$ ,

$$G(x; x^*) = \Phi(x; x^*) + \frac{\mathbf{i}}{4\pi} \int_{-\infty}^{\infty} \frac{\mu(\xi) - |M_-|^{1/2} \alpha_- \mu(\alpha_-^{-1} \xi)}{\mu(\xi)(\mu(\xi) + |M_-|^{1/2} \alpha_- \mu(\alpha_-^{-1} \xi))} e^{\mathbf{i}\mu(\xi)(x_2^* + x_2) + \mathbf{i}\xi(x_1^* - x_1)} d\xi, \quad (20)$$

where  $\Phi(x; x^*) = \frac{\mathbf{i}}{4} H_0^{(1)}(k_0 |x - x^*|)$  appears due to the identity

$$H_0^{(1)}(k_0 |x - x^*|) = \frac{1}{\pi} \int_{-\infty}^{\infty} \frac{1}{\mu(\xi)} e^{\mathbf{i}\mu(\xi)|x_2 - x_2^*| + \mathbf{i}\xi(x_1^* - x_1)} d\xi.$$

Similarly, for  $x \in \mathbb{R}_-^2$ ,

$$G(x; x^*) = G_-(X; x^*) = \frac{\alpha_- \mathbf{i}}{2\pi} \int_{-\infty}^{\infty} \frac{e^{\mathbf{i}\mu(\alpha_- \xi)x_2^* - \mathbf{i}\mu(\xi)X_2 + \mathbf{i}\alpha_- \xi x_1^* - \mathbf{i}\xi X_1}}{\mu(\alpha_- \xi) + |M_-|^{1/2} \alpha_- \mu(\xi)} d\xi, \quad (21)$$

Note that the denominators

$$\mu(\alpha_- \xi) + |M_-|^{1/2} \alpha_- \mu(\xi) \quad \text{and} \quad \mu(\xi) + |M_-|^{1/2} \alpha_- \mu(\alpha_-^{-1} \xi)$$

vanish only when  $\alpha_- = 1$  and  $\xi = \pm k_0$ , in which case the above integrals still exist as Riemann integrals.

For completeness, we give the closed form of  $G$  for  $x^* \in \mathbb{R}_-^2$ . By similar derivations, for  $x \in \mathbb{R}_+^2$ ,

$$G(x; x^*) = \frac{\mathbf{i}}{2\pi} \int_{-\infty}^{\infty} \frac{e^{-\mathbf{i}\mu(\alpha_-^{-1}\xi)X_2^* + \mathbf{i}\alpha_-^{-1}\xi X_1^* + \mathbf{i}\mu(\xi)x_2 - \mathbf{i}\xi x_1}}{|M_-|^{1/2}\alpha_- \mu(\alpha_-^{-1}\xi) + \mu(\xi)} d\xi, \quad (22)$$

and for  $x \in \mathbb{R}_-^2$ ,

$$\begin{aligned} G(x; x^*) = & G_-(X; x^*) = |M_-|^{-1/2} \Phi(X; X^*) \\ & + \frac{\mathbf{i}}{4\pi|M_-|^{1/2}} \int_{-\infty}^{\infty} \frac{\alpha_- \mu(\xi)|M_-|^{1/2} - \mu(\alpha_- \xi)}{\mu(\xi)(\alpha_- \mu(\xi)|M_-|^{1/2} + \mu(\alpha_- \xi))} e^{-\mathbf{i}\mu(\xi)(X_2^* + X_2) + \mathbf{i}\xi(X_1^* - X_1)} d\xi, \end{aligned} \quad (23)$$

where  $X^* = Q_- M_-^{-1/2} x^*$ . From the above formulae, we see that  $G$  satisfies the following reciprocity relation

$$G(x; x^*) = G(x^*; x). \quad (24)$$

The following lemma describes the asymptotic behavior of  $G(x; x^*)$  as  $|x| \rightarrow \infty$ .

**Lemma 3.1.** *For any  $x^* \in \mathbb{R}^2$  with  $x_2^* \neq 0$ , the background Green's function  $G(x; x^*)$  has the following properties:*

(a). *Let  $x^* \in \mathbb{R}_+^2$ . For  $x_2 > 0$ ,*

$$G(x; x^*) = \frac{e^{\mathbf{i}k_0|x|}}{\sqrt{|x|}} [G_\infty^{++}(\beta; x^*) + \mathcal{O}(|x|^{-1})], \quad (25)$$

as  $|x| \rightarrow \infty$ , where  $\beta \in [0, \pi]$  is such that  $x = (|x| \cos \beta, |x| \sin \beta)$  and

$$\begin{aligned} G_\infty^{++}(\beta; x^*) = & \frac{e^{\mathbf{i}\pi/4 - \mathbf{i}k_0 \sin \beta x_2^* - \mathbf{i}k_0 \cos \beta x_1^*}}{\sqrt{8\pi k_0}} \\ & + \frac{e^{\mathbf{i}\pi/4 + \mathbf{i}k_0 \sin \beta x_2^* - \mathbf{i}k_0 \cos \beta x_1^*}}{\sqrt{8\pi k_0}} \frac{k_0 \sin \beta - |M_-|^{1/2} \alpha_- \mu(-\alpha_-^{-1} k_0 \cos \beta)}{k_0 \sin \beta + |M_-|^{1/2} \alpha_- \mu(-\alpha_-^{-1} k_0 \cos \beta)}. \end{aligned}$$

For  $x_2 < 0$ ,

$$G_-(X; x^*) = \frac{e^{\mathbf{i}k_0|X|}}{\sqrt{|X|}} [G_\infty^{-+}(\tilde{\beta}; x^*) + \mathcal{O}(|X|^{-1})], \quad (26)$$

as  $|X| \rightarrow \infty$ , where  $\tilde{\beta} \in [\pi, 2\pi]$  is such that  $X = (|X| \cos \tilde{\beta}, |X| \sin \tilde{\beta})$  and

$$G_\infty^{-+}(\tilde{\beta}; x^*) = \frac{k_0 \sin \tilde{\beta} \alpha_- e^{\mathbf{i}\pi/4 + \mathbf{i}\mu(\alpha_- k_0 \sin \tilde{\beta})x_2^* - \mathbf{i}\alpha_- k_0 \cos \tilde{\beta} x_1^*}}{\sqrt{2\pi k_0} (|M_-|^{1/2} \alpha_- k_0 \sin \tilde{\beta} + \mu(\alpha_- k_0 \cos \tilde{\beta}))}.$$

(b). *Let  $x^* \in \mathbb{R}_-^2$ . For  $x_2 > 0$ ,*

$$G(x; x^*) = \frac{e^{\mathbf{i}k_0|x|}}{\sqrt{|x|}} [G_\infty^{+-}(\beta; x^*) + \mathcal{O}(|x|^{-1})], \quad (27)$$

as  $|x| \rightarrow \infty$ , where

$$G_{\infty}^{+-}(\beta; x^*) = \frac{k_0 \sin \beta e^{i\pi/4 - i\mu(\alpha_- k_0 \sin \beta) X_2^* - i\alpha_-^{-1} k_0 \cos \beta X_1^*}}{\sqrt{2\pi k_0} (k_0 \sin \beta + |M_-|^{1/2} \alpha_- \mu(\alpha_-^{-1} k_0 \cos \beta))},$$

and  $X^* = (X_1^*, X_2^*)^T$ . For  $x_2 < 0$ ,

$$G_-(X; x^*) = \frac{e^{ik_0|X|}}{\sqrt{|X|}} \left[ G_{\infty}^{--}(\tilde{\beta}; x^*) + \mathcal{O}(|X|^{-1}) \right], \quad (28)$$

as  $|X| \rightarrow \infty$ , where

$$G_{\infty}^{--}(\tilde{\beta}; x^*) = \frac{e^{i\pi/4 - ik_0 \sin \tilde{\beta} X_2^* - ik_0 \cos \tilde{\beta} X_1^*}}{\sqrt{8|M_-|\pi k_0}} + \frac{e^{i\pi/4 - ik_0 \sin \tilde{\beta} X_2^* - ik_0 \cos \tilde{\beta} X_1^*}}{\sqrt{8|M_-|\pi k_0}} \frac{|M_-|^{1/2} \alpha_- k_0 \sin \tilde{\beta} - \mu(\alpha_- k_0 \cos \tilde{\beta})}{|M_-|^{1/2} \alpha_- k_0 \sin \tilde{\beta} + \mu(\alpha_- k_0 \cos \tilde{\beta})}.$$

(c).  $G(x; x^*)$  satisfies (RC2).

In the above, the prefactors in the  $\mathcal{O}$ -terms do not depend on  $\beta$  or  $\tilde{\beta}$ .

*Proof.* Based on contour deformations similar to those in the proof of Lemma 2.1 in [13], it is straightforward to verify the above properties.  $\square$

By convention,  $G_{\infty}^{\pm;\pm}$  in the brackets of (25)-(28) constitute the far-field patterns of  $G(x; x^*)$ . Lemma 3.1(c) implies

**Corollary 3.1.** *For any cylindrical incident wave  $u^{\text{inc}}(x; x^*)$  with  $x^* \in \Omega^{\pm}$  and any locally perturbed straight line  $\Gamma$ , (RC1) and (RC2) for the total field  $u^{\text{tot}}(x; x^*)$  are equivalent.*

## 3.2 Plane incident wave

Suppose now  $u^{\text{inc}}(x; \theta) = e^{ik_0(\cos \theta x_1 - \sin \theta x_2)}$  for  $\theta \in (0, \pi)$ . Then, the background solution  $u_b^{\text{tot}}(x; \theta)$  satisfies

$$\Delta u_b^{\text{tot}}(x; \theta) + k_0^2 u_b^{\text{tot}}(x; \theta) = 0, \quad x_2 > 0, \quad (29)$$

$$\Delta_X U_{b,-}^{\text{tot}}(X; \theta) + k_0^2 U_{b,-}^{\text{tot}}(X; \theta) = 0, \quad X_2 < 0, \quad (30)$$

$$u_b^{\text{tot}}(x; \theta) = U_{b,-}^{\text{tot}}(X; \theta), \quad \partial_{x_2} u_b^{\text{tot}}(x; \theta) = \alpha_- \sqrt{|M_-|} \partial_{X_2} U_{b,-}^{\text{tot}}(X; \theta), \quad x_2 = 0 = X_2, \quad (31)$$

where  $U_{b,-}^{\text{tot}}(X; \theta) = u_b^{\text{tot}}(Q_- M_-^{-1/2} X; \theta)$  for  $x_2 < 0$ . By the same approach as above, we obtain

$$u_b^{\text{tot}}(x; \theta) = e^{ik_0(\cos \theta x_1 - \sin \theta x_2)} + \frac{k_0 \sin \theta - |M_-|^{1/2} \mu(\alpha_-^{-1} k_0 \cos \theta) \alpha_-}{k_0 \sin \theta + |M_-|^{1/2} \mu(\alpha_-^{-1} k_0 \cos \theta) \alpha_-} e^{ik_0(\cos \theta x_1 + \sin \theta x_2)}, \quad x \in \mathbb{R}_+^2, \quad (32)$$

$$U_{b,-}^{\text{tot}}(X; \theta) = \frac{2k_0 \sin \theta e^{-i\mu(\alpha_-^{-1}k_0 \cos \theta)X_2 + i\alpha_-^{-1}k_0 \cos \theta X_1}}{k_0 \sin \theta + |M_-|^{1/2} \alpha_- \mu(\alpha_-^{-1}k_0 \cos \theta)}, \quad X \in \mathbb{R}_-^2. \quad (33)$$

Note that to obtain the above formulae, we have implicitly assumed that the reflected and transmitted waves are upgoing and downgoing, respectively.

## 4 Green's representation formula

In this section, we shall use the background Green's function to derive Green's representation formula for a locally perturbed straight line  $\Gamma$ . Let  $\Gamma_T$  denote the boundary of a bounded Lipschitz domain  $\Omega_T$  enclosing the perturbed part of  $\Gamma$ , and let  $\Gamma_T^\pm = \Gamma_T \cap \Omega^\pm$ . Define

$$\nu_c(x) = \begin{cases} \nu(x), & x \in \Gamma_T^+, \\ M_- \nu(x), & x \in \Gamma_T^-, \end{cases}$$

as the conormal vector along  $\Gamma_T$ , where  $\nu(x)$  is the outer unit normal vector of  $\Gamma_T$ . Let  $\Gamma_{N,T}^-$  be the image of the lower part  $\Gamma_T^-$ . We have the following theorem regarding Green's representation formula.

**Theorem 4.1.** *Let  $B_r \subset \Omega_T$  for some sufficiently large  $r > 0$ . A function  $u$  is outgoing in  $\Omega^\pm$  if and only if for  $x \in \mathbb{R}^2 \setminus \overline{\Omega_T}$ ,*

$$u(x) = \int_{\Gamma_T} [\partial_{\nu_c(y)} G(y; x) u(y) - G(y; x) \partial_{\nu_c} u(y)] ds(y), \quad (34)$$

or alternatively,

$$u(x) = \int_{\Gamma_T^+} [\partial_{\nu(y)} G(y; x) u(y) - G(y; x) \partial_{\nu} u(y)] ds(y) + |M_-|^{1/2} \int_{\Gamma_{N,T}^-} [\partial_{\nu^N(Y)} G_-(Y; x) U_-(Y) - G_-(Y; x) \partial_{\nu^N} U_-(Y)] ds(Y), \quad (35)$$

where we recall  $U_-(X) = u(Q_- M_-^{-1/2} X)$  and  $G_-(Y; x) = G(Q_- M_-^{1/2} Y; x)$ ,  $\nu$  denotes the outer unit normal vector of  $\Gamma_T^+$ , and  $\nu^N$  denotes the outer unit normal vector of  $\Gamma_{N,T}^-$ .

*Proof.* We consider the ‘‘only if’’ part as the other part is straightforward by Lemma 3.1. Without loss of generality, we assume  $x \in \Omega^+$ . For sufficiently large  $R > 0$ , let  $\Gamma_R^+ = \partial B_R \cap \Omega^+$  and let  $\Gamma_R^-$  be the preimage of the lower-half circle  $\Gamma_{N,R}^- = \partial B_{\alpha_- R} \cap \mathbb{R}_-^2$ . We choose the boundary  $\partial B_{\alpha_- R}$  since  $\Gamma_R = \Gamma_R^+ \cup \overline{\Gamma_R^-}$  is a closed curve enclosing  $\Gamma_T$ . Let  $\Gamma_{TR}$  be the union of the two line segments on  $\Gamma$  between  $\Gamma_T$  and  $\Gamma_R$ , and  $\Gamma_{N,TR}$  be its image. Green's third identity implies

$$u(x) = \int_{\Gamma_R^+ \cup \Gamma_T^+ \cup \Gamma_{TR}} [G(y; x) \partial_{\nu(y)} u(y) - \partial_{\nu(y)} G(y; x) u(y)] ds(y).$$

On  $\Gamma_{TR}$ ,  $ds(y) = dy_1 = \alpha_-^{-1} dY_1 = \alpha_-^{-1} ds(Y)$  and

$$\partial_{\nu(y)} = -\partial_{y_2} = -\alpha_- |M_-|^{1/2} \partial_{Y_2} = -\alpha_- |M_-|^{1/2} \partial_{\nu^N(Y)},$$

so that

$$\begin{aligned} & \int_{\Gamma_{TR}} [G(y; x) \partial_{\nu(y)} u(y) - \partial_{\nu(y)} G(y; x) u(y)] ds(y) \\ &= -|M_-|^{1/2} \int_{\Gamma_{N,TR}} [G_-(Y; x) \partial_{\nu^N(Y)} U_-(Y) - \partial_{\nu^N(Y)} G(Y; x) U_-(Y)] ds(Y) \\ &= |M_-|^{1/2} \int_{\Gamma_{N,T}^- \cup \Gamma_{N,R}^-} [G_-(Y; x) \partial_{\nu^N(Y)} U_-(Y) - \partial_{\nu^N(Y)} G(Y; x) U_-(Y)] ds(Y). \end{aligned}$$

Taking advantage of the hpSRC (8) in Definition 2.1 and Lemma 3.1, we obtain

$$\begin{aligned} & \int_{\Gamma_R^+} [G(y; x) \partial_{\nu(y)} u(y) - \partial_{\nu(y)} G(y; x) u(y)] ds(y) \\ &+ |M_-|^{1/2} \int_{\Gamma_{N,R}^-} [G_-(Y; x) \partial_{\nu^N(Y)} U_-(Y) - \partial_{\nu^N(Y)} G(Y; x) U_-(Y)] ds(Y) \rightarrow 0, \quad \text{as } R \rightarrow \infty, \end{aligned}$$

by arguing as in the proof of Theorem 2.5 in [10]. Consequently, (35) holds. As for (34), it is straightforward to verify that  $ds(y) \partial_{\nu_c(y)} = |M_-|^{1/2} ds(Y) \partial_{\nu^N(Y)}$  under the change of variable  $Y = Q_- M_-^{-1/2} y$ .  $\square$

Clearly, Theorem 4.1 and Lemma 3.1 explain the reasonability of Definition 2.1 regarding outgoing waves since  $G$  is outgoing in  $\Omega^\pm$ . To conclude this section, we discuss two byproducts of Green's representation formulae (34) and (35). Firstly, the far-field pattern of any outgoing wave can now be well defined. According to the far-field pattern of  $G$  shown in Lemma 3.1, we see immediately that any outgoing wave field  $u$  asymptotically behaves as follows: for  $x = |x|(\cos \beta, \sin \beta) \in \mathbb{R}_+^2$  with  $\beta \in [0, \pi]$ ,

$$u(x) = \frac{e^{ik_0|x|}}{\sqrt{|x|}} \left[ \hat{u}_\infty^+(\beta) + \mathcal{O}\left(\frac{1}{|x|}\right) \right], \quad (36)$$

as  $|x| \rightarrow \infty$ , where

$$\begin{aligned} \hat{u}_\infty^+(\beta) &= \int_{\Gamma_T^+} [\partial_{\nu(y)} G_\infty^{++}(\beta; y) u(y) - G_\infty^{++}(\beta; y) \partial_\nu u(y)] ds(y) \\ &+ |M_-|^{1/2} \int_{\Gamma_{N,T}^-} [\partial_{\nu^N(Y)} G_\infty^{+-}(\beta; Y) U_-(Y) - G_\infty^{+-}(\beta; Y) \partial_{\nu^N} U_-(Y)] ds(Y); \end{aligned}$$

for  $x \in \mathbb{R}_-^2$  so that  $X = Q_- M_-^{-1/2} x = |X|(\cos \tilde{\beta}, \sin \tilde{\beta})$  with  $\tilde{\beta} \in [\pi, 2\pi]$ ,

$$u(x) = \frac{e^{ik_0|X|}}{\sqrt{|X|}} \left[ \hat{u}_\infty^-(\tilde{\beta}) + \mathcal{O}\left(\frac{1}{|X|}\right) \right], \quad (37)$$

as  $|X| \rightarrow \infty$ , where

$$\begin{aligned} \hat{u}_\infty^-(\tilde{\beta}) &= \int_{\Gamma_T^+} \left[ \partial_{\nu(y)} G_\infty^{-+}(\tilde{\beta}; y) u(y) - G_\infty^{-+}(\tilde{\beta}; y) \partial_\nu u(y) \right] ds(y) \\ &\quad + |M_-|^{1/2} \int_{\Gamma_{N,T}^-} \left[ \partial_{\nu(Y)} G_\infty^{--}(\tilde{\beta}; Y) U_-(Y) - G_\infty^{--}(\tilde{\beta}; Y) \partial_{\nu N} U_-(Y) \right] ds(Y). \end{aligned}$$

Consequently,  $\hat{u}_\infty^+(\beta)$  and  $\hat{u}_\infty^-(\tilde{\beta})$  can be defined as the far-field pattern of the outgoing field  $u$ .

Secondly, the unbounded domain can now be truncated onto  $\Omega_T$ . Let  $x$  approach  $\Gamma_T$  in (34), we obtain the following transparent boundary condition (TBC)

$$(\mathcal{I} - \mathcal{K}_b)[u](x) = -\mathcal{S}_b[\partial_{\nu_c} u](x) \quad (38)$$

on  $\Gamma_T$ , where  $\mathcal{I}$  is the identity operator such that  $\mathcal{I}[u] = u$ , and  $\mathcal{K}_b$  and  $\mathcal{S}_b$  are two boundary integral operators on  $\Gamma_T$  defined as follows: for any  $x \in \Gamma_T$  and  $\psi \in C^\infty(\Gamma_T)$ ,

$$\mathcal{S}_b[\psi](x) := 2 \int_{\Gamma_T} G(y; x) \psi(y) ds(y), \quad (39)$$

$$\mathcal{K}_b[\psi](x) := 2 \text{p.v.} \int_{\Gamma_T} \partial_{\nu_c(y)} G(y; x) \psi(y) ds(y), \quad (40)$$

where p.v. indicates Cauchy principal value. In our scattering problem, according to the radiation conditions (RC1) and (RC2),  $u$  can represent  $u^{\text{tot}} - u_b^{\text{tot}}$  or  $u^{\text{tot}}$  depending on the type of the incident wave.

Theoretically, the TBC (38) plays a central role in proving the well-posedness of the scattering problem (4) and (5) under the radiation condition (RC1) or (RC2), but unfortunately, classical methods coupling TBCs to variational formulations [12] break down here. This is because that the integral operators  $\mathcal{S}_b$  and  $\mathcal{K}_b$  lose properties such as strong ellipticity and compactness. In a subsequent work [14], we shall present a new framework to establish the well-posedness theory.

Numerically, one may incorporate any standard numerical method with (38) to compute  $u^{\text{tot}}$  on the bounded domain  $\Omega_T$  by properly discretizing the two integral operators  $\mathcal{S}_b$  and  $\mathcal{K}_b$ . Nevertheless, it becomes essential to develop a fast and accurate algorithm to evaluate  $G$  and its derivatives. If one does not wish to use the TBC (38) in a numerical method, then an artificial boundary condition must be developed, as shall be discussed in the next section.

## 5 Regionalized PML and BIE method

In this section, we shall propose a stable RPML to truncate  $\Omega^\pm$ , and shall develop a high-accuracy BIE method to numerically compute  $u^{\text{tot}}$ . Unless otherwise indicated, we shall assume the incident wave to be the plane wave  $u^{\text{inc}}(x; \theta)$ . For simplicity, we shall suppress the argument  $\theta$ .

## 5.1 Governing equations

Let  $u_{\pm}^{\text{og}} = u^{\text{og}}|_{\Omega^{\pm}}$  be the two outgoing waves in  $\Omega^{\pm}$  according to (RC1). Then,  $u_{\pm}^{\text{og}}$  satisfy

$$\nabla \cdot (M_{\pm} \nabla u_{\pm}^{\text{og}}) + k_0^2 u_{\pm}^{\text{og}} = 0, \quad \text{on } \Omega^{\pm}, \quad (41)$$

$$u_{+}^{\text{og}}(x) - u_{-}^{\text{og}}(x) = \lim_{y \rightarrow x^{-}} u_b^{\text{tot}}(y) - \lim_{y \rightarrow x^{+}} u_b^{\text{tot}}(y), \quad x \in \Gamma, \quad (42)$$

$$\partial_{\nu_c} u_{+}^{\text{og}}(x) - \partial_{\nu_c} u_{-}^{\text{og}}(x) = \lim_{y \rightarrow x^{-}} \partial_{\nu_c} u_b^{\text{tot}}(y) - \lim_{y \rightarrow x^{+}} \partial_{\nu_c} u_b^{\text{tot}}(y), \quad x \in \Gamma, \quad (43)$$

where we now set  $\nu(x)$  to be the unit normal vector of  $\Gamma$  at  $x$  pointing towards  $\Omega^{-}$ ,  $\nu_c = M\nu$ , and  $x^{\pm}$  indicate one-sided limits taken from  $\Omega^{\pm}$ , respectively. Note that  $u_b^{\text{tot}}(x)$  should be defined as (32) for  $x \in \Omega^{+}$  and (33) for  $x \in \Omega^{-}$  even if  $x$  is outside of one of the two domains  $\mathbb{R}_{\pm}^2$ , so that (41) holds.

Recall the assumption  $M_{+} = I_2$  and the change of coordinates  $X = Q_{-} M_{-}^{-1/2} x$ . Let  $U_{-}^{\text{og}}(X) = u_{-}^{\text{og}}(M_{-}^{-1/2} Q_{-}^T X)$ ,  $\Omega_{N}^{-}$  be the image of  $\Omega^{-}$ , and  $\Gamma_N = \partial\Omega_{N}^{-}$ . Then, (41)-(43) become

$$\Delta u_{+}^{\text{og}}(x) + k_0^2 u_{+}^{\text{og}}(x) = 0, \quad x \in \Omega^{+}, \quad (44)$$

$$\Delta_X U_{-}^{\text{og}} + k_0^2 U_{-}^{\text{og}} = 0, \quad X \in \Omega_{N}^{-}, \quad (45)$$

$$u_{+}^{\text{og}}(x) - U_{-}^{\text{og}}(X) = F(x), \quad x \in \Gamma, \quad (46)$$

$$\partial_{\nu(x)} u_{+}^{\text{og}}(x) + \gamma(x) \partial_{\nu^N(X)} U_{-}^{\text{og}}(X) = G(x), \quad x \in \Gamma, \quad (47)$$

where we now set  $\nu^N(X)$  to be the unit normal vector of  $\Gamma_N$  pointing away from  $\Omega_{N}^{-}$ ,  $\gamma(x) = |M_{-}|^{1/2} \frac{ds(X)}{ds(x)}$ ,  $ds(x)$  and  $ds(X)$  represent the differential arc lengths of  $\Gamma$  at point  $x$  and  $\Gamma_N$  at the corresponding point  $X$ , respectively, and

$$F(x) = \lim_{Y \rightarrow X^{-}} U_{b,-}^{\text{tot}}(Y) - \lim_{y \rightarrow x^{+}} u_b^{\text{tot}}(y),$$

$$G(x) = -\gamma(x) \lim_{Y \rightarrow X^{-}} \partial_{\nu^N(Y)} U_{b,-}^{\text{tot}}(Y) - \lim_{y \rightarrow x^{+}} \partial_{\nu(x)} u_b^{\text{tot}}(y).$$

In particular, if  $x$  is away from the perturbed part of  $\Gamma$ ,  $\gamma(x) = |M_{-}|^{1/2} \alpha_{-}$  and (31) indicates that  $F(x) = G(x) = 0$  so that in fact  $F$  and  $G$  are compactly supported of supports the same as the perturbed part of  $\Gamma$ . According to the asymptotic behavior (36) and (37) for outgoing waves at infinity, we expect that  $u_{\pm}^{\text{og}}$  and  $U_{-}^{\text{og}}$  can be perfectly absorbed by two separately defined PMLs, as shall be discussed in the next subsection.

## 5.2 Regionalized perfectly matched layers

As  $\Omega^{+}$  and  $\Omega_{N}^{-}$  have different coordinate systems, we introduce an RPML technique to complexify the coordinates of  $x$  and  $X$ . As indicated by its name, the RPML should be defined regionally and hence is no longer uniaxial. Let  $l_i$ ,  $L_i$ ,  $d_i$ , and  $D_i$  be positive constants for  $i = 1, 2$ . As shown in Figure 2,  $\Omega_{\text{RPML}}^{+} = \Omega^{+} \cap \{x : |x_1| < l_1 + d_1, |x_2| < l_2 + d_2\}$ ,  $\Omega_{N,\text{RPML}}^{-} = \Omega_{N}^{-} \cap \{X : |X_1| < L_1 + D_1, |X_2| < L_2 + D_2\}$ , and  $\Omega_{\text{RPML}}^{-}$  be the preimage of  $\Omega_{N,\text{RPML}}^{-}$ . We choose  $l_i$  and  $L_i$  to be sufficiently large

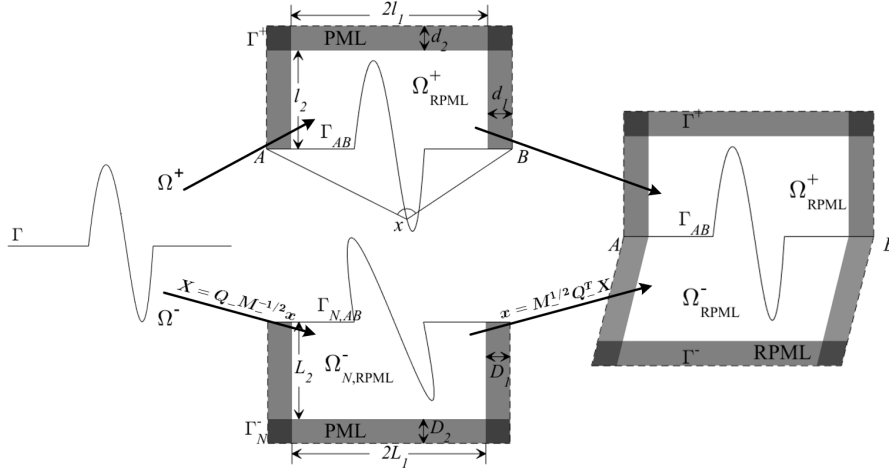


Figure 2: The setup of an RPML: rectangular PMLs are setup both in  $\Omega^+$  and in  $\Omega_N^-$ , the image of  $\Omega^-$ ;  $\Omega_{\text{RPML}}^+$  and  $\Omega_{N,\text{RPML}}^-$  are the truncated regions;  $\Omega_{\text{RPML}}^-$ , the preimage of  $\Omega_{N,\text{RPML}}^-$ , is slanted due to the change of coordinates.

such that  $\Omega_{\text{RPML}}^+ \cup \Omega_{\text{RPML}}^-$  enclose the perturbed part of  $\Gamma$ . Let  $\Gamma^+ = \partial\Omega_{\text{RPML}}^+ \setminus \Gamma$ ,  $\Gamma_N^- = \partial\Omega_{N,\text{RPML}}^- \setminus \Gamma_N$ , and  $\Gamma^-$  be the preimage of  $\Gamma_N^-$ . For  $x = (x_1, x_2)^T$  in the top region  $\Omega^+$ , we define

$$\tilde{x}_i = x_i + \mathbf{i} \int_0^{x_i} \sigma_i(t) dt, \quad i = 1, 2, \quad (48)$$

where the two functions  $\sigma_i(x)$  are positive for  $|x_i| \in [l_i, l_i + d_i]$ , and are zero elsewhere. For  $X = (X_1, X_2)^T$  in the bottom region  $\Omega_N^-$ , the image of  $\Omega^-$ , we define

$$\tilde{X}_i = X_i + \mathbf{i} \int_0^{X_i} \sigma_i^N(t) dt, \quad i = 1, 2, \quad (49)$$

where the two functions  $\sigma_i^N(X)$  are positive for  $|X_i| \in [L_i, L_i + d_i]$ , and are zero elsewhere. The regions with nonzero  $\sigma_i$  or nonzero  $\sigma_i^N$  are called the RPML regions, as indicated by the shaded regions in Figure 2. Thus,  $d_i$  and  $D_i$  represent the thicknesses of the RPML.

Let  $\tilde{x} = (\tilde{x}_1, \tilde{x}_2)^T$  for  $x \in \Omega^+$ , and  $\tilde{X} = (\tilde{X}_1, \tilde{X}_2)^T$  for  $X \in \Omega_N^-$ . Analogous to Green's function in a layered isotropic medium in [8], the background Green's function  $G(x; \cdot)$  can be analytically extended to well define  $G(\tilde{x}; \cdot)$  for  $x \in \Omega_{\text{RPML}}^+$  and  $G_-(\tilde{X}; \cdot)$  for  $X \in \Omega_{N,\text{RPML}}^-$ . By the reciprocity relation (24) and Green's representation formula (35), analytic continuation also applies for  $u_+^{\text{og}}$  and  $U_-^{\text{og}}$  so that  $\tilde{u}_+^{\text{og}}(x) = u_+^{\text{og}}(\tilde{x})$  and  $\tilde{U}_-^{\text{og}}(X) = U_-^{\text{og}}(\tilde{X})$  are well-defined. By the chain rule, we obtain

$$\nabla \cdot (\mathbf{A} \nabla \tilde{u}_+^{\text{og}}) + k_0^2 J \tilde{u}_+^{\text{og}} = 0, \quad \text{in } \Omega^+, \quad (50)$$

$$\nabla_X \cdot (\mathbf{A}_N \nabla_X \tilde{U}_-^{\text{og}}) + k_0^2 J_N \tilde{U}_-^{\text{og}} = 0, \quad \text{in } \Omega_N^-, \quad (51)$$

where  $q_i = 1 + \mathbf{i}\sigma_i(x)$ ,  $q_i^N = 1 + \mathbf{i}\sigma_i^N(X)$ ,  $\mathbf{A} = \text{Diag}\{q_2/q_1, q_1/q_2\}$ ,  $\mathbf{A}_N = \text{Diag}\{q_2^N/q_1^N, q_1^N/q_2^N\}$ ,  $J = q_1(x)q_2(x)$  and  $J_N = q_1^N(X)q_2^N(X)$ .

Across the interface  $\Gamma$  or  $\Gamma_N$ , we expect that the interface conditions (42) and (43) should be continued to inside the RPML. This relies on the following condition

$$\sigma_1^N(X_1) = \sigma_1(x_1), \quad x_1 \in \mathbb{R}, \quad (52)$$

as indicated by the following lemma.

**Lemma 5.1.** *Under the condition (52), the interface conditions (46) and (47) can be analytically continued to*

$$\tilde{u}_+^{\text{og}}(x) - \tilde{U}_-^{\text{og}}(X) = F(x), \quad (53)$$

$$\partial_{\nu(x)} \tilde{u}_+^{\text{og}}(x) + \gamma(x) \partial_{\nu^N(X)} \tilde{U}_-^{\text{og}}(X) = G(x), \quad (54)$$

for any  $x \in \Gamma$  and  $X = Q_- M_-^{-1/2} x \in \Gamma_N$ .

*Proof.* Outside the RPML region, (53) and (54) are exactly the same as (46) and (47). Inside the RPML region,  $\Gamma$  coincides with  $x_2 = 0$  so that  $X_1 = \alpha_- x_1$ ,  $\nu(x) = (0, -1)^T$ ,  $\nu^N(X) = (0, 1)^T$ , and  $F(x) = G(x) \equiv 0$ . Condition (52) directly implies that on  $x_2 = 0$ ,

$$\tilde{X}_1 = X_1 + \int_0^{X_1} \sigma_1^N(t) dt = \alpha_- x_1 + \int_0^{\alpha_- x_1} \sigma_1(t/\alpha_-) dt = \alpha_- \tilde{x}_1,$$

so that  $\tilde{x} = M_-^{1/2} Q_-^T \tilde{X}$ . Since  $F(x) = 0$ , the interface condition (46) reduces to

$$U_-^{\text{og}}(X) = u_+^{\text{og}}(M_-^{1/2} Q_-^T X).$$

The identity theorem for analytic functions directly implies

$$U_-^{\text{og}}(\tilde{X}) = u_+^{\text{og}}(M_-^{1/2} Q_-^T \tilde{X}) = u_+^{\text{og}}(\tilde{x}).$$

Equation (54) can be proved similarly.  $\square$

Now, we directly truncate  $\tilde{u}_+^{\text{og}}$  and  $\tilde{U}_-^{\text{og}}$  onto  $\Omega_{\text{RPML}}^+$  and  $\Omega_{N, \text{RPML}}^-$  respectively by imposing the following Dirichlet boundary conditions

$$\tilde{u}_+^{\text{og}} = 0, \quad \text{on } \Gamma^+, \quad (55)$$

$$\tilde{U}_-^{\text{og}} = 0, \quad \text{on } \Gamma_N^-. \quad (56)$$

Since  $u_+^{\text{og}}$  and  $U_-^{\text{og}}$  are purely outgoing waves at infinity, the artificial boundary conditions (55) and (56) are expected to induce a truncation error that decays exponentially as the RPML parameters  $d_i$ ,  $D_i$ ,  $\sigma_i$  and  $\sigma_i^N$  for  $i = 1, 2$  increase, as shall be illustrated by the numerical examples in Section 6. According to (52), we take

$$L_1 = \alpha_- l_1, \quad D_1 = \alpha_- d_1, \quad (57)$$

so that along  $\Gamma$ ,  $\tilde{u}_+^{\text{og}}$  and  $\tilde{U}_-^{\text{og}}$  enter the RPML and terminate simultaneously. Consequently, equations (50), (51), (53), (54), (55) and (56) form a closed boundary value problem for the two unknowns  $\tilde{u}_+^{\text{og}}$  and  $\tilde{U}_-^{\text{og}}$ . In the next subsection, we shall adopt a previously developed BIE method to numerically solve this boundary value problem.

### 5.3 The PML-based BIE method

As indicated by Figure 2, let  $\Gamma_{AB}$  be the truncated part of  $\Gamma$  by  $\Omega_{\text{RPML}}^+$  with the two endpoints  $A$  and  $B$  and  $\Gamma_{N,AB}$  be the truncated part of  $\Gamma_N$  by  $\Omega_{N,\text{RPML}}^-$ . It can be seen from (57) that  $\Gamma_{N,AB}$  is the image of  $\Gamma_{AB}$ . We first consider  $\tilde{u}_+^{\text{og}}$  in  $\Omega_{\text{RPML}}^+$ . For any given function  $g \in H^{-1/2}(\Gamma_{AB})$ , consider the following boundary value problem

$$\nabla \cdot (\mathbf{A} \nabla \tilde{u}_+^{\text{og}}) + k_0^2 J \tilde{u}_+^{\text{og}} = 0, \quad \text{on } \Omega_{\text{RPML}}^+, \quad (58)$$

$$\tilde{u}_+^{\text{og}} = 0, \quad \text{on } \partial\Omega_{\text{RPML}}^+ \setminus \Gamma, \quad (59)$$

$$\partial_{\nu_c} \tilde{u}_+^{\text{og}}|_{\Gamma_{AB}} = g \in H^{-1/2}(\Gamma_{AB}), \quad (60)$$

where the conormal vector  $\nu_c = \mathbf{A}^T \nu$ . Fredholm theory indicates that this problem has a unique solution  $\tilde{u}_+^{\text{og}} \in H^1(\Omega_{\text{RPML}}^+)$  except for  $k_0$  in a countable set of eigenfrequencies; numerically, such eigenfrequencies can be easily avoided by adjusting  $\Gamma_{AB}$  or the aforementioned RPML parameters. Then, we are able to define a Neumann-to-Dirichlet map  $\mathcal{N}_{AB}^+ : H^{-1/2}(\Gamma_{AB}) \rightarrow \tilde{H}^{1/2}(\Gamma_{AB})$  such that  $\tilde{u}_+^{\text{og}}|_{\Gamma_{AB}} = \mathcal{N}_{AB}^+ \partial_{\nu_c} \tilde{u}_+^{\text{og}}|_{\Gamma_{AB}}$ . Following [15] closely, we develop a high-accuracy BIE method to numerically approximate  $\mathcal{N}_{AB}^+$ .

The fundamental solution of (58) is

$$\tilde{\Phi}(x; y) = \Phi(\tilde{x}; \tilde{y}) = \frac{\mathbf{i}}{4} H_0^{(1)}[k_0 \rho(\tilde{x}, \tilde{y})], \quad (61)$$

where  $\tilde{y} = (\tilde{y}_1, \tilde{y}_2)$  and the complexified distance function  $\rho$  is defined to be

$$\rho(\tilde{x}, \tilde{y}) = [(\tilde{x}_1 - \tilde{y}_1)^2 + (\tilde{x}_2 - \tilde{y}_2)^2]^{1/2}. \quad (62)$$

According to [15], we have the following Green's representation formula

$$\begin{aligned} \tilde{u}_+^{\text{og}}(x) &= \int_{\partial\Omega_{\text{RPML}}^+} \{\tilde{\Phi}(x; y) \partial_{\nu_c} \tilde{u}_+^{\text{og}}(y) - \partial_{\nu_c} \tilde{\Phi}(x; y) \tilde{u}_+^{\text{og}}(y)\} ds(y) \\ &\approx \int_{\Gamma_{AB}} \{\tilde{\Phi}(x; y) \partial_{\nu_c} \tilde{u}_+^{\text{og}}(y) - \partial_{\nu_c} \tilde{\Phi}(x; y) \tilde{u}_+^{\text{og}}(y)\} ds(y), \end{aligned} \quad (63)$$

for all  $x \in \Omega_1^+$ . Here, we have assumed that on the RPML boundary  $\Gamma^+$ , the co-normal derivative  $\partial_{\nu_c} \tilde{u}_+^{\text{og}} \approx 0$ , since we expect that the RPML can absorb the outgoing wave  $\tilde{u}_+^{\text{og}}$  completely. An alternative way to obtain (63) is regarding itself as a direct truncation of the following integral

$$\tilde{u}_+^{\text{og}}(x) = \int_{\Gamma} \{\tilde{\Phi}(x; y) \partial_{\nu_c} \tilde{u}_+^{\text{og}}(y) - \partial_{\nu_c} \tilde{\Phi}(x; y) \tilde{u}_+^{\text{og}}(y)\} ds(y), \quad (64)$$

which does not involve the complexification of  $y_2$ .

As  $x$  approaches  $\Gamma_{AB}$ , the jump relations for single- and double-layer potentials imply [15, Eq. (42)]

$$\mathcal{K}_{AB}[\tilde{u}_+^{\text{og}}](x) - \mathcal{K}_{0,AB}[1](x) \tilde{u}_+^{\text{og}}(x) \approx \mathcal{S}_{AB}[\partial_{\nu_c} \tilde{u}_+^{\text{og}}](x), \quad (65)$$

where we have defined the following boundary integral operators on  $\Gamma_{AB}$ ,

$$\mathcal{S}_{AB}[\phi](x) = 2 \int_{\Gamma_{AB}} \tilde{\Phi}(x; y) \phi(y) ds(y), \quad (66)$$

$$\mathcal{K}_{AB}[\phi](x) = 2 \text{ p.v. } \int_{\Gamma_{AB}} \partial_{\nu_c} \tilde{\Phi}(x; y) \phi(y) ds(y), \quad (67)$$

$$\mathcal{K}_{0,AB}[\phi](x) = -\angle AxB/\pi + 2 \text{ p.v. } \int_{\Gamma_{AB}} \partial_{\nu_c} \tilde{\Phi}_0(x; y) \phi(y) ds(y), \quad (68)$$

where the angle  $\angle AxB$  is indicated in Figure 2, and

$$\tilde{\Phi}_0(x; y) = -\frac{1}{2\pi} \log \rho(\tilde{x}, \tilde{y}), \quad (69)$$

is the fundamental solution of the complexified Laplace equation

$$\nabla \cdot (\mathbf{A} \nabla \tilde{u}) = 0. \quad (70)$$

Roughly speaking,  $\tilde{u}_+^{\text{og}}|_{\Gamma_{AB}} \approx (\mathcal{K}_{AB} - \mathcal{K}_{0,AB}[1])^{-1} \mathcal{S}_{AB} \partial_{\nu_c} \tilde{u}_+^{\text{og}}|_{\Gamma_{AB}}$  so that the NtD operator  $\mathcal{N}_{AB}^+ \approx (\mathcal{K}_{AB} - \mathcal{K}_{0,AB}[1])^{-1} \mathcal{S}_{AB}$ .

Suppose the piecewise smooth curve  $\Gamma_{AB}$  is parameterized by  $\{x(s) = (x_1(s), x_2(s)) \mid 0 \leq s \leq L\}$ , where  $s$  is the arclength parameter. Since corners may exist,  $\tilde{u}_+^{\text{og}}(x(s))$  can have corner singularities in its derivatives at corners. To smoothen  $\tilde{u}_+^{\text{og}}$ , we introduce a grading function  $s = w(t)$ ,  $0 \leq t \leq 1$ . For a smooth segment of  $\Gamma_{AB}$  corresponding to  $s \in [s^0, s^1]$  and  $t \in [t^0, t^1]$  such that  $s^i = w(t^i)$  for  $i = 0, 1$ , where  $s^0$  and  $s^1$  correspond to two corners, we take [10, Eq. (3.104)]

$$s = w(t) = \frac{s^0 w_1^p + s^1 w_2^p}{w_1^p + w_2^p}, \quad t \in [t^0, t^1], \quad (71)$$

where the positive integer  $p$  ensures that the derivatives of  $w(t)$  vanish at the corners up to order  $p$ ,

$$w_1 = \left( \frac{1}{2} - \frac{1}{p} \right) \xi^3 + \frac{\xi}{p} + \frac{1}{2}, \quad w_2 = 1 - w_1, \quad \xi = \frac{2t - (t^0 + t^1)}{t^1 - t^0}.$$

To simplify the notation, we shall use  $x(t)$  to denote  $x(w(t))$ , and  $x'(t)$  to denote  $\frac{dx}{ds}(w(t))w'(t)$  in the following. Assume that  $[0, 1]$  is uniformly sampled by  $N_{\text{tot}}$  grid points  $\{t_j = jh\}_{j=1}^{N_{\text{tot}}}$  with even  $N_{\text{tot}}$  and grid size  $h = 1/N_{\text{tot}}$  and that the grid points contain all the corner points. Thus,  $\mathcal{S}_{AB}[\partial_{\nu_c} \tilde{u}_+^{\text{og}}]$  at point  $x = x(t_j)$  can be parameterized by

$$\mathcal{S}_{AB}[\partial_{\nu_c} \tilde{u}_+^{\text{og}}](x(t_j)) = \int_0^1 S(t_j, t) \psi^s(t) dt, \quad (72)$$

where  $S(t_j, t) = \frac{i}{2} H_0^{(1)}(k\rho(x(t_j), x(t)))$ , and the scaled co-normal vector  $\psi_+^s(t) = \partial_{\nu_c} \tilde{u}_+^{\text{og}}(x(t)) |x'(t)|$ , smoother than  $\partial_{\nu_c} \tilde{u}_+^{\text{og}}(x(t))$ , is introduced to regularize the approximation of  $\mathcal{N}_{AB}$ .

Considering the logarithmic singularity of  $S(t_j, t)$  at  $t = t_j$ , we can discretize the integral in (72) by Alpert's 6th-order hybrid Gauss-trapezoidal quadrature rule [1] and then by trigonometric interpolation to get

$$\mathcal{S}_{AB}[\partial_{\nu_c} \tilde{u}_+^{\text{og}}] \begin{bmatrix} x(t_1) \\ \vdots \\ x(t_{N_{\text{tot}}}) \end{bmatrix} \approx \mathbf{S}_{AB} \begin{bmatrix} \psi_+^s(t_1) \\ \vdots \\ \psi_+^s(t_{N_{\text{tot}}}) \end{bmatrix}, \quad (73)$$

where the  $N_{\text{tot}} \times N_{\text{tot}}$  matrix  $\mathbf{S}_{AB}$  approximates  $\mathcal{S}_{AB}$ . One similarly approximates  $\mathcal{K}_{AB}[\tilde{u}_+^{\text{og}}](x(t_j))$  and  $\mathcal{K}_{0,AB}[1](x(t_j))$  for  $j = 1, \dots, N_{\text{tot}}$ , so that we obtain on  $\Gamma_{AB}$  that

$$\mathbf{u}_+^{\text{og}} \approx \mathbf{N}_{AB}^+ \boldsymbol{\psi}_+^s, \quad (74)$$

where  $\mathbf{u}_+^{\text{og}}$  and  $\boldsymbol{\psi}_+^s$  represent  $N_{\text{tot}} \times 1$  column vectors of  $\tilde{u}_+^{\text{og}}$  and  $\psi_+^s$  at the  $N_{\text{tot}}$  grid points of  $\Gamma_{AB}$ , respectively, and  $\mathbf{N}_{AB}^+$  represents an  $N_{\text{tot}} \times N_{\text{tot}}$  matrix approximating  $\mathcal{N}_{AB}^+$ .

Now consider  $\tilde{U}_-^{\text{og}}$  in  $\Omega_{N,\text{RPML}}^-$ . Let  $\nu_c^N = \mathbf{A}_N \nu^N$  and  $\Psi_-^s(t) = \partial_{\nu_c^N} \tilde{U}_-^{\text{og}}(X(t)) |X'(t)|$ , where  $X(t)$  parameterizing  $\Gamma_{N,AB}$  is the image of  $x(t)$ . Following the same procedure as above, one obtains

$$\mathbf{U}_-^{\text{og}} \approx \mathbf{N}_{AB}^- \boldsymbol{\Psi}_-^s, \quad (75)$$

where  $\mathbf{U}_-^{\text{og}}$  and  $\boldsymbol{\Psi}_-^s$  represent  $N_{\text{tot}} \times 1$  column vectors of  $\tilde{U}_-^{\text{og}}$  and  $\Psi_-^s$  at  $N_{\text{tot}}$  grid points of  $\Gamma_{N,AB}$ , respectively, and  $\mathbf{N}_{AB}^-$  is an  $N_{\text{tot}} \times N_{\text{tot}}$  matrix relating to the NtD operator mapping  $\partial_{\nu_c^N} \tilde{U}_-^{\text{og}}$  to  $\tilde{U}_-^{\text{og}}$ . To match the two equations (74) and (75) on  $\Gamma_{AB}$ , the  $N_{\text{tot}}$  grid points of  $\Gamma_{N,AB}$  must be the image of the  $N_{\text{tot}}$  grid points of  $\Gamma_{AB}$ . Consequently, (53) and (54) imply

$$\begin{bmatrix} \mathbf{N}_{AB}^+ & -\mathbf{N}_{AB}^- \\ \mathbf{I}_{N_{\text{tot}}} & \mathbf{D}_{N_{\text{tot}}} \end{bmatrix} \begin{bmatrix} \boldsymbol{\psi}_+^s \\ \boldsymbol{\Psi}_-^s \end{bmatrix} = \begin{bmatrix} \mathbf{F} \\ \mathbf{G} \end{bmatrix}, \quad (76)$$

where  $\mathbf{I}_{N_{\text{tot}}}$  is the  $N_{\text{tot}} \times N_{\text{tot}}$  identity matrix,  $\mathbf{D}_{N_{\text{tot}}} = \text{Diag}\{\gamma(x(t_1)), \dots, \gamma(x(t_{N_{\text{tot}}}))\}$ ,  $\mathbf{F}$  and  $\mathbf{G}$  are two  $N_{\text{tot}} \times 1$  vectors consist of elements  $F(x(t_j))$  and  $G(x(t_j)) |w'(t_j)| q_1(x_1(t_j))$ , respectively. Here, equation (54) is multiplied by  $|w'(t_j)| q_1(x_1(t_j))$  due to the relation between  $\psi_+^s$  and  $\partial_{\nu_c} u_+^{\text{og}}$ .

Solving the above linear system, we get  $\boldsymbol{\psi}_+^s$  and  $\boldsymbol{\Psi}_-^s$  on  $\Gamma_{AB}$  and  $\Gamma_{N,AB}$ , respectively, and hence obtain  $\mathbf{u}_+^{\text{og}}$  and  $\mathbf{U}_-^{\text{og}}$  by (74) and (75). Green's representation formula (63) then applies to get  $\tilde{u}_+^{\text{og}}$  in  $\Omega_{\text{RPML}}^+$  and  $\tilde{U}_-^{\text{og}}$  in  $\Omega_{N,\text{RPML}}^-$ . Consequently,  $u^{\text{og}}$  and hence  $u^{\text{tot}}$  become available in the physical regions of  $\Omega_{\text{RPML}}^+ \cup \Omega_{\text{RPML}}^-$ , where we recall that  $\Omega_{\text{RPML}}^-$  is the preimage of  $\Omega_{N,\text{RPML}}^-$ .

## 5.4 Uniqueness of the orthogonal matrix $Q_-$ and failure of the uniaxial PML

To conclude this section, we discuss in the change of coordinates  $X = Q_- M_-^{-1/2} x$ , the reason why the orthogonal matrix  $Q_-$  should be chosen as in (7). From a numerical perspective, such a choice is significantly essential in the design of the RPML and is the only choice that makes the RPML stable.

To illustrate this, we first give a formal proof on the failure of a uniaxial PML (UPML), the instability of which for homogeneous and orthotropic background has been shown in [2]. In the UPML, the coordinate transformation (48) applies in both  $\Omega^+$  and  $\Omega^-$ . Then, we can define the UPML regions  $\Omega_{\text{UPML}}^\pm = \{x : |x_1| \leq l_1 + d_1, \pm x_2 < l_2 + d_2\} \cap \Omega^\pm$ . Let  $\Omega_{\text{UPHY}}^\pm$  and  $\Omega_{\text{RPHY}}^\pm$  be the physical regions of  $\Omega_{\text{UPML}}^\pm$  and  $\Omega_{\text{RPML}}^\pm$ , respectively. Note that  $\Omega_{\text{UPML}}^+ = \Omega_{\text{RPML}}^+$  and  $\Omega_{\text{UPHY}}^+ = \Omega_{\text{RPHY}}^+$ . Let  $\tilde{u}_{\pm, \text{UPML}}^{\text{og}}$  denote the UPML-truncated wave field in  $\Omega_{\text{UPML}}^\pm$ . Following the same procedure of the PML-based BIE method, we obtain a linear system for unknowns  $\partial_{\nu_c} \tilde{u}_{\pm, \text{UPML}}^{\text{og}}$  on

$\Gamma$ . As the interface conditions are only defined on  $\Gamma$ , such a linear system should give rise to  $\tilde{u}_{-, \text{UPML}}^{\text{og}}(x) = \tilde{U}_-^{\text{og}}(X)$  and  $\partial_{\nu_c} \tilde{u}_{-, \text{UPML}}^{\text{og}}(x) = |M_-|^{1/2} \partial_{\nu_c^N} \tilde{U}_-^{\text{og}}(X) ds(X) / ds(x)$  for any  $x \in \Gamma$ .

Now, for any  $x \in \Omega_{\text{UPHY}}^- \cap \Omega_{\text{RPML}}^-$ , the common physical region of the UPML and the RPML, Green's representation formula, analogous to (64), implies

$$\tilde{u}_{-, \text{UPML}}^{\text{og}}(x) = \int_{\Gamma} \{ \tilde{\Phi}_{\text{UPML}}(x; y) \partial_{\nu_c} \tilde{u}_{-, \text{UPML}}^{\text{og}}(y) - \partial_{\nu_c(y)} \tilde{\Phi}_{\text{UPML}}(x; y) \tilde{u}_{-, \text{UPML}}^{\text{og}}(y) \} ds(y),$$

where  $\tilde{\Phi}_{\text{UPML}}(x; y) = \Phi_{\text{UPML}}(\tilde{x}; \tilde{y})$  and

$$\Phi_{\text{UPML}}(x; y) = |M_-|^{-1/2} \Phi(Q_- M_-^{-1/2} x; Q_- M_-^{-1/2} y)$$

is the fundamental solution of (4) for  $M(x) \equiv M_-$ . By the change of variable  $Y = Q_- M_-^{-1/2} y$ ,

$$\begin{aligned} \tilde{u}_{-, \text{UPML}}^{\text{og}}(x) &= \int_{\Gamma_N} \{ \Phi(Q_- M_-^{-1/2} x; \tilde{Y}) \partial_{\nu_c^N} \tilde{U}_-^{\text{og}}(Y) - \partial_{\nu_c^N(Y)} \Phi(Q_- M_-^{-1/2} x; \tilde{Y}) \tilde{U}_-^{\text{og}}(Y) \} ds(Y) \\ &= \int_{\Gamma_N} \{ \Phi(X; \tilde{Y}) \partial_{\nu_c^N} \tilde{U}_-^{\text{og}}(Y) - \partial_{\nu_c^N(Y)} \Phi(X; \tilde{Y}) \tilde{U}_-^{\text{og}}(Y) \} ds(Y). \end{aligned} \quad (77)$$

On the other hand,

$$\tilde{U}_-^{\text{og}}(X) = \int_{\Gamma_N} \{ \Phi(\tilde{X}; \tilde{Y}) \partial_{\nu_c^N} \tilde{U}_-^{\text{og}}(Y) - \partial_{\nu_c^N} \Phi(\tilde{X}; \tilde{Y}) \tilde{U}_-^{\text{og}}(Y) \} ds(Y). \quad (78)$$

Thus,  $\tilde{u}_{-, \text{UPML}}^{\text{og}}(x) = \tilde{U}_-^{\text{og}}(X)$  since  $\tilde{X} = X$ . It is surprising that the unstable UPML can unexpectedly provide accurate solutions in part of its physical domain based on the proposed BIE method!

However, the situation changes considerably when  $x \in \Omega_{\text{UPHY}}^- \setminus \overline{\Omega_{\text{RPML}}^-}$ . Equation (78) can still be analytically and stably continued to evaluate  $\tilde{U}_-^{\text{og}}(X)$  although  $X$  now is in the RPML region of  $\Omega_{\text{RPML}}^-$ . On the contrary, (77), computable though, cannot be analytically continued to the region  $\Omega_{\text{UPHY}}^- \setminus \overline{\Omega_{\text{RPML}}^-}$  as the branch cut of  $\Phi(X; \tilde{Y})$ ,  $\{X : \rho^2(X, \tilde{Y}) < 0\}$ , is crossed definitely. For example, if  $Y_1 = X_1$ ,  $\tilde{Y}_1$  has a sufficiently large imaginary part, and  $X_2$  is sufficiently close to  $Y_2$ , then

$$\rho^2(X, \tilde{Y}) = (X_1 - \tilde{Y}_1)^2 + (X_2 - Y_2)^2 < 0.$$

Consequently,  $\tilde{u}_{-, \text{UPML}}^{\text{og}}(x)$  can not be an analytic function in  $\Omega_{\text{UPHY}}^-$ . But it contradicts our expectation that in the physical region  $x \in \Omega_{\text{UPHY}}^-$ ,  $\tilde{u}_{-, \text{UPML}}^{\text{og}}(x)$  coincides with  $u^{\text{og}}(x)$ , which must be analytic. We note that if numerical methods such as finite difference or finite element methods are used, then much worse numerical solutions are expected. The incorrectly enforced zero boundary condition on the UPML boundary  $\partial\Omega_{\text{UPML}}^- \setminus \Gamma$  makes the truncation error propagate back to the whole computational domain!

In a similar fashion to the above, it can be seen that choosing  $Q_-$  other than a scalar multiple of (7) does not work either. Different from the UPML, a different choice of  $Q_-$  leads to a rotation of the RPML region of  $\Omega_{\text{RPML}}^-$ . Again, branch cut

of  $\Phi$  appears inside the corresponding physical region, making such an RPML not work either.

To illustrate the above statements more clearly, we consider a specific example below. Let  $\Gamma = \{x : x_2 = 0\}$ ,  $k_0 = 2\pi$ ,  $\epsilon^+$  is the  $3 \times 3$  identity matrix  $I_3$ , and

$$\epsilon^- = \begin{bmatrix} 4 & 3 & 0 \\ 3 & 9 & 0 \\ 0 & 0 & 1 \end{bmatrix}.$$

We compute  $u^{\text{tot}}(x; x^*)$  for a cylindrical incident wave  $u^{\text{inc}}(x; x^*)$  excited by a source at  $x^* = (0, 0.1)^T$  based on three different types of PMLs: (1) UPML; (2) RPML-I with  $Q_- = I_2$ ; (3) RPML-II with  $Q_-$  defined in (7). In  $\Omega^+$ , we let  $l_1 = 1$  and  $d_1 = 1$  so that  $\Gamma_{AB} = \{x : |x_1| < 2, x_2 = 0\}$ , and choose (79) with  $S = 2$  to complexify  $x_1$  in  $\Omega^+$  and  $X_1$  in  $\Omega_N^-$ . The computation domain is set to be  $\Omega_D = (-2, 2) \times (-2, 2)$ , and we let  $l_2$  and  $L_2$  sufficiently large so that  $\Omega_D$  contains only regions that complexify  $x_1$ . To obtain sufficiently accurate numerical solutions, we discretize  $\Gamma_{AB}$  by  $N_{\text{tot}} = 800$  points.

Clearly,  $u_{\text{exa}}^{\text{tot}}(x; x^*) = G(x; x^*)$  defined in (20) and (21) is the exact solution. Let  $\tilde{u}_{\text{UPML}}^{\text{tot}}$ ,  $\tilde{u}_{\text{RPML},1}^{\text{tot}}$ , and  $\tilde{u}_{\text{RPML},2}^{\text{tot}}$  be the three numerical solutions produced by UPML, RPML-I and RPML-II. Real parts of the exact solution and the three numerical solutions are shown in Figure 3. In comparison with the exact solution, the errors

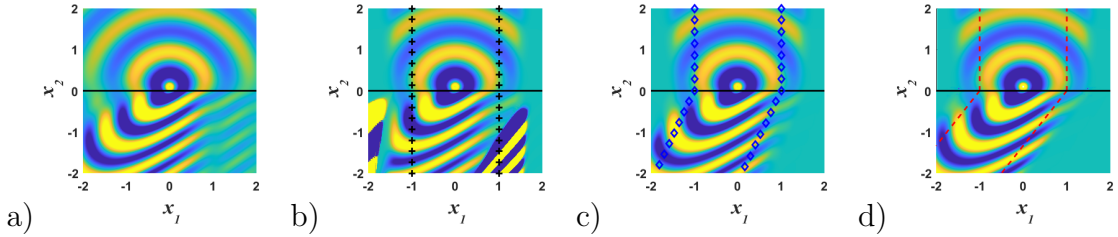


Figure 3: Performance of different PMLs: a) Exact solution  $u_{\text{exa}}^{\text{tot}}$ ; b) UPML solution  $\tilde{u}_{\text{UPML}}^{\text{tot}}$  with PML entrances marked by '+'s; c) RPML-I solution  $\tilde{u}_{\text{RPML},1}^{\text{tot}}$  with entrances marked by 'o's; d) RPML-II solution  $\tilde{u}_{\text{RPML},2}^{\text{tot}}$  with entrances marked by dashed lines.

of the three numerical solutions are depicted in Figure 4. As can be seen, only

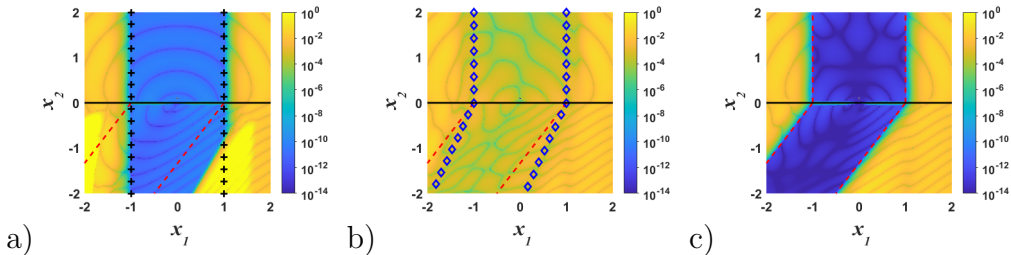


Figure 4: Errors of the three numerical solutions: a)  $\tilde{u}_{\text{UPML}}^{\text{tot}}$ ; b)  $\tilde{u}_{\text{RPML},1}^{\text{tot}}$ ; c)  $\tilde{u}_{\text{RPML},2}^{\text{tot}}$ . Dashed lines in all figures indicate the entrance of the RPML-II. The '+'s indicate the entrance of the UPML, whereas the 'o's indicate the entrance of the RPML-I.

$\tilde{u}_{\text{RPML},2}^{\text{tot}}$  perfectly coincides with the exact solution  $u_{\text{exa}}^{\text{tot}}$  in its physical region with pointwise errors around  $\mathcal{O}(10^{-12})$ . In contrast,  $\tilde{u}_{\text{UPML}}^{\text{tot}}$  and  $\tilde{u}_{\text{RPML},1}^{\text{tot}}$  are accurate only in the two common regions between their physical regions and the physical region of RPML-II, as expected according to the above theory.

## 6 Numerical examples

In this section, we carry out several numerical experiments to validate the stability of the RPML and to illustrate the high accuracy of the proposed BIE method. In all examples, we let the freespace wavelength  $\lambda = 1$  so that  $k_0 = 2\pi$ ,  $\epsilon^+ = I_3$ , and

$$\epsilon^- = \begin{bmatrix} 4 & 1 & 0 \\ 1 & 9 & 0 \\ 0 & 0 & 1 \end{bmatrix}.$$

In the setup of the RPML, we choose

$$\sigma_1^N(X_1) = \sigma_1(x_1) = \begin{cases} \frac{2Sf_1^6}{f_1^6 + f_2^6}, & l_1 \leq x_1 \leq l_1 + d_1; \\ \sigma_1(-x_1), & -l_1 - d_1 \leq x_1 \leq l_1; \\ 0, & \text{elsewhere,} \end{cases} \quad (79)$$

where

$$f_1 = \left(\frac{1}{2} - \frac{1}{p}\right) \bar{x}_1^3 + \frac{\bar{x}_1}{p} + \frac{1}{2}, \quad f_2 = 1 - f_1, \quad \bar{x}_1 = \frac{x_1 - (l_1 + d_1)}{d_1},$$

and  $S > 0$  determines the RPML strength for absorbing outgoing waves. The function  $\sigma_1$  is of class  $C^6$  at  $x_1 = \pm l_1$ , so that  $(\pm l_1, 0)^T$  can be considered as smooth points of  $\Gamma_{AB}$ . We point out that  $\sigma_2$  and  $\sigma_2^N$  are useless in the computations. We choose  $p = 6$  to define the grading function  $s = w(t)$  in (71). In each example, to quantify the truncation error due to the RPML, we evaluate the relative error

$$E_{\text{rel}} = \frac{\|\mathbf{u}_{\text{num}}^{\text{tot}} - \mathbf{u}_{\text{exa}}^{\text{tot}}\|_{\infty}}{\|\mathbf{u}_{\text{exa}}^{\text{tot}}\|_{\infty}},$$

where  $\mathbf{u}_{\text{num}}^{\text{tot}}$  denotes the vector of a numerical solution  $u_{\text{num}}^{\text{tot}}$  for the total field  $u^{\text{tot}}$  at grid points of the perturbed part of  $\Gamma$ , and  $\mathbf{u}_{\text{exa}}^{\text{tot}}$  denotes the vector of a reference solution  $u_{\text{exa}}^{\text{tot}}$ , the exact solution of the total field  $u^{\text{tot}}$  if available or a sufficiently accurate numerical solution, at the same grid points.

**Example 1.** In this example, we assume again that  $\Gamma = \{x : x_2 = 0\}$  to check the performance of our RPML and the convergence order of the PML-based BIE method. Here,  $l_1 = 1$  and the PML thickness in  $\Omega^+$  is fixed as  $d_1 = 1$  so that  $\Gamma_{AB} = \{x \in \Gamma : |x_1| < 2\}$  with  $A = (-2, 0)^T$  and  $B = (2, 0)^T$ .

We consider only a cylindrical incident wave excited by a source located at  $x^* = (0, 0.1)^T$ . The exact solution is the Green's function  $G(x; x^*)$  given by (20) and (21). The ‘‘perturbed’’ part on  $\Gamma$  is assumed to be  $\{x : |x_1| < 1, x_2 = 0\}$ , i.e., the physical part of  $\Gamma_{AB}$ . As shown in Figure 5, the computational domain  $\Omega_{\text{PHY}}$  is set to be the union of a rectangular region above  $x_2 = 0$ , and a slanted region

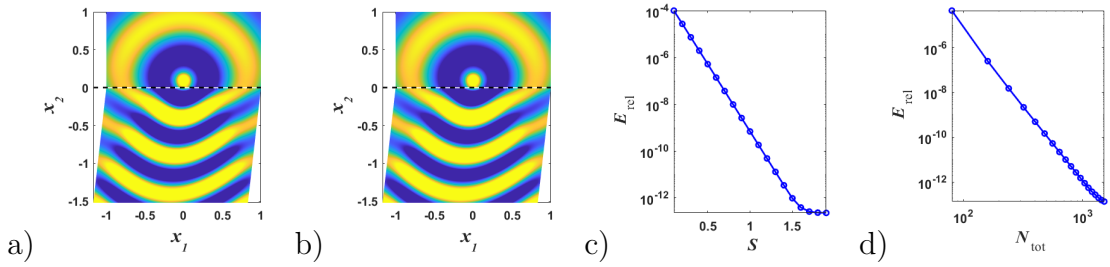


Figure 5: Example 1: a) Exact solution  $u_{\text{exa}}^{\text{tot}}$ ; b) Numerical solution  $u_{\text{num}}^{\text{tot}}$ ; c)  $E_{\text{rel}}$  against  $S$ ; d)  $E_{\text{rel}}$  against  $N_{\text{tot}}$ . Dashed lines in a) and b) indicate the interface  $\Gamma$ .

below  $x_2 = 0$  since the physical region of  $\Omega_{\text{RPML}}^-$  is always slanted. By choosing  $N_{\text{tot}} = 1600$  grid points on  $\Gamma_{AB}$ , we compute  $u_{\text{num}}^{\text{tot}}$  on  $\Omega_{\text{PHY}}$ , and compare it with the exact solution  $u_{\text{exa}}^{\text{tot}}$ . Figure 5 (a) and (b) show the real parts of  $u_{\text{exa}}^{\text{tot}}$  and  $u_{\text{num}}^{\text{tot}}$  in  $\Omega_{\text{PHY}}$ . It can be seen that the two are distinguishable.

To show the stability of the RPML, we fix  $N_{\text{tot}} = 1600$  and compute the relative error  $E_{\text{rel}}$  for different values of  $S$ , ranging from 0.1 to 2. The results are shown in Figure 5(c), where only the vertical axis is logarithmically scaled. We observe that  $E_{\text{rel}}$  decays exponentially at the beginning and then yields to the discretization error which dominates the relative error when  $S$  becomes large. Next, we study  $E_{\text{rel}}$  against  $N_{\text{tot}}$  for  $S = 2$ . For  $N_{\text{tot}}$  ranging from 80 to 1520 of step size 80, the relative errors are depicted in Figure 5(d) where both axes are logarithmically scaled. The slope of the decreasing part of the curve reveals that the convergence order of the PML-based BIE method is approximately seven. We observe that the numerical solutions are accurate to at least 12 significant digits.

**Example 2.** In this example, we assume that the perturbed part of  $\Gamma$  consists of two connected semicircles of radius 1, as shown by the dashed lines in Figure 6.

We consider two types of incidences, a plane incident wave  $u^{\text{inc}}(x; \theta) = e^{ik_0(\cos \theta x_1 - \sin \theta x_2)}$  with  $\theta = \frac{\pi}{3}$  and a cylindrical incident wave excited by a source at the point  $x^* = (1, 1)^T$ . Here,  $\Gamma_{AB}$  consists of four smooth segments. We choose  $S = 2$ ,  $l_1 = 1.5$ ,  $d_1 = 1.5$ , and 800 points on each smooth segment so that  $N_{\text{tot}} = 3200$ , to compute a reference solution  $u_{\text{exa}}^{\text{tot}}$  for either of the two incidences. Real parts of the two reference solutions are shown in Figure 6 (a) and (b). Note that the computational domain is still slanted below  $x_2 = 0$ .

With the reference solutions available for the two incident waves, we show the stability of the RPML. We fix  $N_{\text{tot}} = 3200$ , and check the relation between the relative error  $E_{\text{rel}}$  and one of the two RPML parameters  $d_1$  and  $S$  with the other one fixed. For  $d_1 = 1.5$ , the relative error  $E_{\text{rel}}$  against  $S$ , ranging from 0.1 to 1.5 is shown in Figure 6(c). For  $S = 2$ , the relative error  $E_{\text{rel}}$  against  $d_1$ , ranging from 0.1 to 1.2, is shown in Figure 6(d). The vertical axes in both figures are logarithmically scaled. We observe from the decaying lines that  $E_{\text{rel}}$  decays exponentially as either  $S$  or  $d_1$  increases for both the two incident waves. The convergence curves indicate that the numerical solutions are accurate to at least 11 significant digits.

**Example 3.** In the last example, we assume that  $\Omega^+$  contains three indentations, each of which is a square of size 1, as shown by the dashed line in Figure

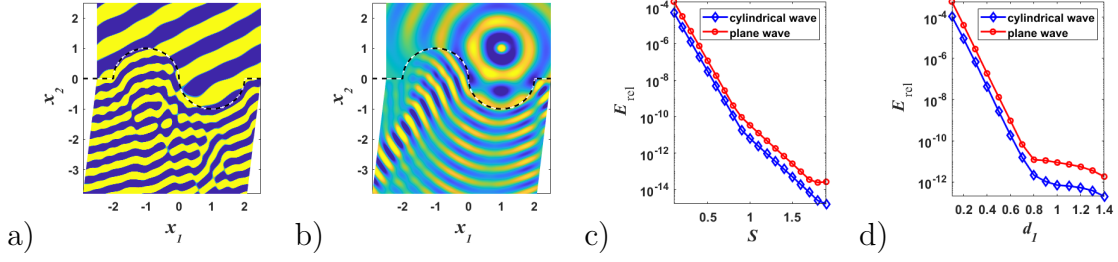


Figure 6: Example 2: a) Reference solution for a plane incident wave of angle  $\theta = \pi/3$ ; b) Reference solution for a cylindrical incident wave excited by a source at  $x^* = (1, 1)^T$ ; c)  $E_{\text{rel}}$  against  $S$ ; d)  $E_{\text{rel}}$  against  $d_1$ . Dashed lines in a) and b) indicate the interface  $\Gamma$ .

7.

We consider two types of incidences, a plane incident wave  $u^{\text{inc}}(x; \theta) = e^{ik_0(\cos \theta x_1 - \sin \theta x_2)}$  with  $\theta = \frac{\pi}{3}$  and a cylindrical incident wave excited by a source at  $x^* = (0, 1)^T$ . We choose  $S = 4$ ,  $l_1 = 3.5$ ,  $d_1 = 1.5$ , and 200 points on each of the 13 smooth segments of  $\Gamma_{AB}$  so that  $N_{\text{tot}} = 2600$ , to compute a reference solution  $u_{\text{exa}}^{\text{tot}}$  for either of the two incidences. Real parts of the two reference solutions are shown in Figure 7 (a) and (b).

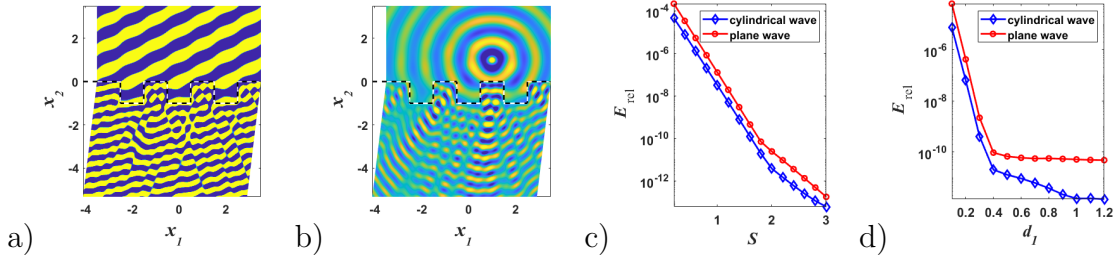


Figure 7: Example 3: a) Reference solution for a plane incident plane wave of incident angle  $\theta = \pi/3$ ; b) Reference solution for a cylindrical incident wave excited by  $x^* = (0, 1)^T$ ; c)  $E_{\text{rel}}$  against  $S$ ; d)  $E_{\text{rel}}$  against  $d_1$ . Dashed lines in a) and b) indicate the interface  $\Gamma$ .

With the reference solutions available, we show the stability of the RPML now. We fix  $N_{\text{tot}} = 2600$ , and check the relation between the relative error  $E_{\text{rel}}$  and one of the two RPML parameters  $d_1$  and  $S$ . For  $d_1 = 1.5$ , the relative error  $E_{\text{rel}}$  against  $S$ , ranging from 0.2 to 3.0, is shown in Figure 6(c). For  $S = 4$ , the relative error  $E_{\text{rel}}$  against  $d_1$ , ranging from 0.1 to 1.2, is shown in Figure 6(d). We observe from the two figures that  $E_{\text{rel}}$  decays exponentially as either  $S$  or  $d_1$  increases for both the two incident waves. The convergence curves indicate that the numerical solutions are accurate to at least 10 significant digits. The solutions are less accurate compared with the previous examples, since  $\Gamma$  contains more corners and each smooth segment is discretized by much less number of grid points.

## 7 Conclusion

In this paper, we studied wave scattering in a two-layer orthotropic medium in two dimensions. A novel SRC condition was proposed and a stable RPML technique was developed to truncate the unbounded domain. The resulting boundary value problem was solved by a recently developed PML-based BIE method [15]. Numerical experiments have justified the accuracy of the numerical method and the stability of the RPML method, showing that the truncation error due to the RPML decays exponentially as the RPML parameters increase.

As we can see from the numerical results, due to the transition matrix  $Q_- M_-^{-1/2}$ , the physical region of the computational domain always contains a slanted region. If the slanted region is too narrow, then the resulting computational domain will be too small making numerical solutions probably useless in practice. A possible remedy could be using more generalized complexifications of  $x_1$  and  $X_1$  to enlarge the physical domain [4]. We shall investigate this issue in a future work. Besides, we shall rigorously prove the well-posedness of the scattering problem and shall justify the exponentially decaying truncation error due to the RPML in the subsequent work [14]. Moreover, our RPML technique exhibits deep potential in terminating waves in more complicated anisotropic backgrounds. Thus, it is of great interests to investigate the extension of the RPML to more general anisotropic media for both electro-magnetic and elastic waves in the future.

## Acknowledgements

W. L. would like to express his sincere gratitude to Prof. Anne-Sophie Bonnet-Ben Dhia for sharing her slides, originally presented in the conference of WAVES 2019 in Vienna, which greatly inspires the current work.

## References

- [1] B. K. Alpert. Hybrid Gauss-trapezoidal quadrature rules. *SIAM Journal on Scientific Computing*, 20(5):1551–1584, 1999.
- [2] E. Bécache, S. Fauqueux, and P. Joly. Stability of perfectly matched layers, group velocities and anisotropic waves. *J. Comput. Phys.*, 188:399–433, 2003.
- [3] J.-P. Berenger. A perfectly matched layer for the absorption of electromagnetic waves. *J. Comput. Phys.*, 114(2):185 – 200, 1994.
- [4] A.-S. Bonnet-Ben Dhia, S. N. Chandler-Wilde, S. Fliss, C. Hazard, K.-M. Perfekt, and Y. Tjandrawidjaja. The complex-scaled half-space matching method. *SIAM J. Math. Anal.*, to appear, 2021.
- [5] A.-S. Bonnet-Ben Dhia, S. Fliss, and A. Tonnoir. The halfspace matching method: A new method to solve scattering problems in infinite media. *J. Comput. Appl. Math.*, 338:44–68, 2018.

- [6] W. Cai. *Computational Methods for Electromagnetic Phenomena*. Cambridge University Press, New York, NY, 2013.
- [7] Z. Chen and H. Wu. An adaptive finite element method with perfectly matched absorbing layers for the wave scattering by periodic structures. *SIAM J. Numer. Anal.*, 41(3):799–826, 2003.
- [8] Z. Chen and W. Zheng. Convergence of the uniaxial perfectly matched layer method for time-harmonic scattering problems in two-layered media. *SIAM J. Numer. Anal.*, 48:2158–2185, 2010.
- [9] W. C. Chew. *Waves and fields in inhomogeneous media*. IEEE PRESS, New York, 1995.
- [10] D. Colton and R. Kress. *Inverse Acoustic and Electromagnetic Scattering Theory (3rd Edition)*. Springer, 2013.
- [11] D. Colton, R. Kress, and P. Monk. Inverse scattering from an orthotropic medium. *J. Comput. Appl. Math.*, 81:269–298, 1997.
- [12] G. Hu, W. Lu, and A. Rathsfeld. Time-harmonic acoustic scattering from locally-perturbed periodic curves. *SIAM J. Appl. Math.*, to appear, 2021.
- [13] W. Lu. Mathematical analysis of wave radiation by a step-like surface. *SIAM J. Appl. Math.*, 81(2):666–693, 2021.
- [14] W. Lu. Wave scattering in layered orthotropic media II: well-posedness and PML theory. *to be submitted*, 2021.
- [15] W. Lu, Y. Y. Lu, and J. Qian. Perfectly matched layer boundary integral equation method for wave scattering in a layered medium. *SIAM J. Appl. Math.*, 78(1):246–265, 2018.
- [16] W. Lu, Y. Y. Lu, and D. Song. A numerical mode matching method for wave scattering in a layered medium with a stratified inhomogeneity. *SIAM J. Sci. Comput.*, 41(2):B274–B294, 2019.
- [17] P. Monk. *Finite Element Methods for Maxwell’s Equations*. Oxford University Press, 2003.
- [18] E. A. Skelton, S. D. M Adams, and R. V. Craster. Guided elastic waves and perfectly matched layers. *Wave motion*, 44(7):573–592, 2007.
- [19] A. Toflove and S. C. Haganess. *Computational Electrodynamics: The Finite Difference Time Domain Method, Second Editions*. Artech House, Norwood, MA, 2000.
- [20] A. Tonnoir. *Conditions transparentes pour la diffraction d’ondes en milieu élastique anisotrope*. PhD thesis, École Polytechnique, 2015.

- [21] X. Yu, G. Hu, W. Lu, and A. Rathsfeld. PML and high-accuracy boundary integral equation solver for wave scattering by a locally defected periodic surface. *submitted, arXiv:2108.00897*, 2021.